



Imad El Chiti,¹ Shadi Najjar,² George Saad,¹ and Salah Sadek¹

Experimental Setup for Measuring p-y Curves of Rigid Walls Supporting Granular Backfill

Reference

I. El Chiti, S. Najjar, G. Saad, and S. Sadek, "Experimental Setup for Measuring p-y Curves of Rigid Walls Supporting Granular Backfill," *Geotechnical Testing Journal* 46, no. 1 (January/February 2023): 104–131. <https://doi.org/10.1520/GTJ20220084>

ABSTRACT

In the context of performance-based design, there is interest in quantifying the relationship between the lateral earth pressure and the wall displacement using the concept of p-y curves. Although p-y curves have been extensively used in the analysis of piles, their use in the analysis of rigid walls is still in its early stages. There is a need for realistic and simplified models that could describe the p-y relationship for rigid walls to be used as input in robust soil-structure-interaction analyses. This paper aims at studying the development of lateral stresses behind rigid walls in the context of p-y curves using a laboratory-scale retaining wall prototype that is 0.5 m wide, 1.2 m high, and 2.6 m long. The main objective is to provide insight on the p-y response behind rigid walls under static and cyclic loading conditions for different backfill densities and confinement conditions. Results indicate that the proposed experimental setup yields repeatable and consistent measurements of the p-y response, which was found to be highly nonlinear and not adequately represented by the simple elastic-perfectly plastic model that was adopted in the literature in modeling soil-structure interaction between basement walls and sand backfill. Unique results from the cyclic tests indicated a process of densification that dominated the volumetric tendency of the sand during cyclic loading, with the p-y curves showing a significant increase in stiffness and maximum pressure at the passive side after 10 loading cycles. The gradual increase in stiffness decreased with the number of cycles until convergence in the passive stiffness was observed after 9 to 10 cycles.

Keywords

p-y curves, sand, passive pressure, active pressure, rigid walls

Manuscript received January 1, 2022; accepted for publication September 22, 2022; published online November 23, 2022. Issue published January 1, 2023.

¹ Department of Civil and Environmental Engineering, American University of Beirut, PO Box 11-0236, Bliss St., Beirut, Riad ElSolh 1107-2020, Lebanon

² Department of Civil and Environmental Engineering, American University of Beirut, PO Box 11-0236, Bliss St., Beirut, Riad ElSolh 1107-2020, Lebanon (Corresponding author), e-mail: sn06@aub.edu.lb, <https://orcid.org/0000-0003-1824-4540>

Introduction

The mobilization of lateral stresses behind retaining walls constitutes a typical soil-structure-interaction problem. For structures with underground basement walls, the interaction between the adjacent soil and the walls affects the response of the system, particularly under cyclic loading conditions. In the context of performance-based design, there has been interest in quantifying the relationship between the lateral earth pressure and the wall displacement by using the p-y curve method, which aims at replacing the homogeneous soil continuum by a series of springs that mimic the soil behavior. For the particular case of buildings with underground basements, the use of p-y curves is to replace the soil behind the basement walls by springs that could be used by the structural engineer to quantify the response of the structure (e.g., base shear, interstory drift, modal analysis, etc.) under static and cyclic loading conditions that may or may not push the soil to the active or passive limit state. Replacing the soil with springs that are modeled with realistic p-y curves eliminates the need for computationally expensive full-fledged finite element analyses that would require a full numerical model for both the structure and the soil behind the walls.

The p-y method has been advocated for and applied by geotechnical and structural engineers in the design of laterally loaded piles. However, the use of p-y curves for the analysis of rigid retaining walls is still in its early stages. There is a need for realistic and simplified models that could describe the p-y relationship for rigid walls to be used as input in robust soil-structure-interaction analyses. The experimental setup presented in this paper is a step that would lead to the understanding of the p-y response that is needed to model these springs.

The earlier investigations on p-y curves for laterally loaded piles involved experimental tests for piles embedded in clay (Matlock 1970) and sand (Reese, Cox, and Koop 1974). These earlier works targeted the effect of cyclic loading on the resulting p-y response for piles in clay and sand, respectively. The problem of laterally loaded piles has since been extensively studied using full scale field tests, centrifuge tests, and 3-D finite element analyses. Conversely, very limited studies have been conducted on the mobilization of lateral earth pressure behind rigid walls in the context of p-y curves.

Published experimental investigations that studied the lateral earth pressure response behind rigid retaining walls are summarized in **Table 1** (Tsagareli 1965; Fang and Ishibashi 1986; Take and Valsangkar 2001; Fang, Ho, and Chen 2002; Dave and Dasaka 2012; Gutberlet, Katzenbach, and Hutter 2013; Khosravi, Pipatpongsa, and Takemura 2013; Patel and Deb 2020). A detailed investigation of the experimental setups used in previous studies indicates the following limitations:

- All 1-g model tests involved walls with relatively small heights (less than 70 cm), with three out of the five tests involving a translational movement that may not apply to the case of basement walls. The only two tests that involved rotation around the base were restricted to medium dense sand (no effect of density), and one of them involved a surcharge.
- The only centrifuge test in **Table 1** (Take and Valsangkar 2001) focused on the at-rest response with no data collected for passive and active movements.
- The results of the only full-scale test in **Table 1** (Tsagareli 1965) were restricted to the “resultant” active lateral force and did not show the variation of the lateral earth pressure with wall displacement (p-y response) at different depths.
- The results from the only comprehensive study that presented active p-y curves for loose and medium sand under different displacement conditions (Fang and Ishibashi 1986) were conducted on a shaking table and may not represent the static p-y response.
- None of the published experimental studies show any results for cyclic p-y curves in the active and passive directions.

The novelty of the current study is that it addresses the limitations of previous experimental work by investigating the p-y response of rigid walls under active and passive conditions, different backfill relative densities, and more importantly, for static and cyclic loading.

TABLE 1

Summary of published experimental studies involving walls supporting sand

Reference	Type of Test	Prototype Dimensions			Type of Sand	Wall Movement	Output
		H, cm	W, cm	L, cm			
Tsagareli (1965)	Full scale test	200–400	110–360	NA	Loose	Active	Resultant lateral force
Fang and Ishibashi (1986)	1 g shaking table	104	102	240	Loose to medium	RB, RT, T. Active	Lateral stress vs. wall rotation or translation
Take and Valsangkar (2001)	Centrifuge 35.7 g	14	25.4	1.5–18	Loose and dense	At rest	Lateral stress vs. depth
Fang, Ho, and Chen (2002)	1 g model test	55	100	200	Loose, medium and dense	T. Passive	Lateral stress vs. depth at wall displacements
Dave and Dasaka (2012)	1 g model test	70	30.5	90	Medium	RB. Active/passive	Lateral stress vs. depth with surcharge
Gutberlet, Katzenbach, and Hutter (2013)	1 g model test	22.5	72	90	Loose and very dense (layered)	T. Passive	Lateral force vs. wall displacement
Khosravi, Pipatpongsa, and Takemura (2013)	1 g model test	30	20	22	Loose	T. Active	Lateral stress vs. wall displacement
Patel and Deb (2020)	1 g model test	60	140	180	Medium	RB. Active	Lateral stress vs. wall displacement

Note: H = height; L = length; NA = not applicable; RB = rotation about the base; RT = rotation about top; T = translation; W = weight.

In the absence of comprehensive experimental full-scale studies that target the p-y response of walls under monotonic and cyclic loading, semiempirical p-y models have been used in the literature for investigating the structural response of buildings with basement walls. Briaud and Kim (1998) were the first to recommend p-y relationships for the analysis and design of tie-back walls. These p-y relationships were calibrated/back calculated using data collected from full scale tests on tie-back walls in sand (not rigid walls). Briaud and Kim (1998) state that the lateral earth pressure that is exerted by the soil on the wall is bounded by the active and passive earth pressure conditions. Based on the data collected, they recommend that the active earth pressure could be assumed to be mobilized at outward wall movements of 1.3 mm (away from the retained soil), whereas the passive resistance could be mobilized at a wall movement of 13 mm (into the retained soil). El Ganainy and El Naggari (2009) and Saad, Najjar, and Saddik (2016) adopted this p-y relationship as the “backbone curve” for the lateral pressure–lateral deflection relationship used for modeling the embedding soil in their analysis of the response of buildings with underground basements. Richards, Huang, and Fishman (1999) also recommended that the soil be modeled by a series of springs having a bilinear p-y curve consisting of an elastic portion bounded by upper and lower limits defined by the active and passive states, with the recommended elastic stiffness that defines the p-y response being a function of the square root of depth.

In reality, the relationship between lateral earth pressure and wall displacement is expected to be complex, nonlinear, and affected by the height of the wall, the relative density of the backfill material, the interface friction between the wall and the soil, the nonlinearity of the soil response, and the type of wall movement (translation and/or rotation). In an attempt to study the complexities associated with modeling the p-y response, Elchiti et al. (2017) and El-Chiti et al. (2018) utilized a 2-D finite element model in PLAXIS to investigate the static/monotonic soil-structure interaction between rigid walls and a sand backfill for active states of loading while enforcing a realistic model of the soil support at the base of the wall. The main goal was to identify and characterize the components of the p-y relationship at different depths with particular emphasis on the effects of the interface friction angle between the wall and the soil. The results of the numerical simulations showed that the static p-y response was highly nonlinear, depth dependent, and sensitive to the interface friction coefficient, wall height, and density of the sand.

The main goal of the work presented herein is to provide a first step toward a comprehensive investigation of the p-y response of granular soils that are supported by rigid retaining walls over the full range of wall

displacements (active to passive) and under both monotonic and cyclic loading conditions. This goal is achieved experimentally by designing and constructing a laboratory-scale retaining wall prototype that is rotated around its base to measure the p-y response for granular soils under monotonic and cyclic loading conditions. The conceived and built experimental setup is presented in this paper, along with preliminary results that were obtained from monotonic and cyclic tests conducted on a wall supporting loose, medium, and dense sand. The results are presented in the form of stress-displacement curves recorded at different depths along the height of the wall.

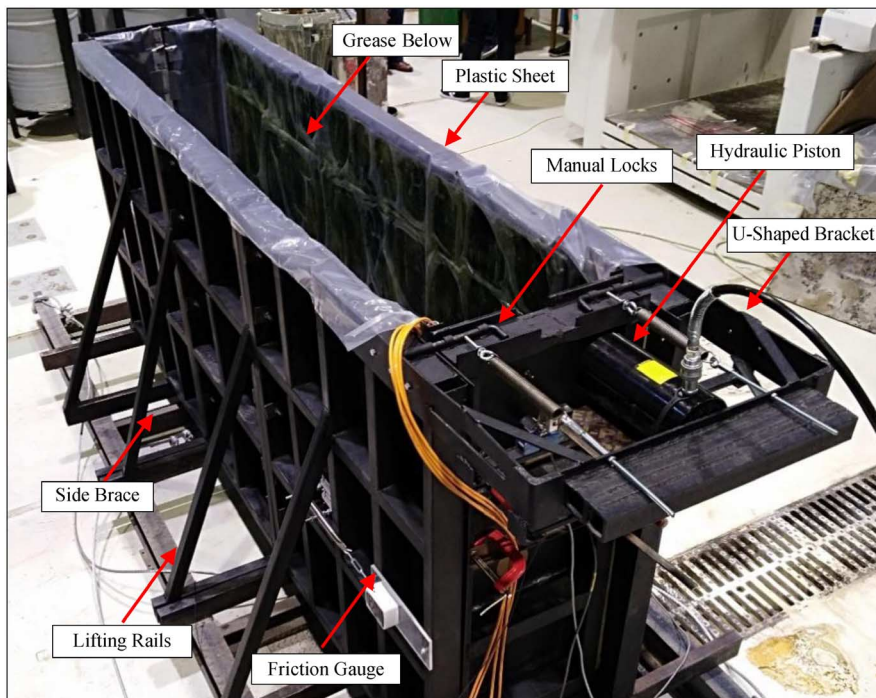
Experimental Setup

A steel soil retaining system that can carry 2.5 tons (24.5 kN) of sand was designed and constructed in the laboratory for the purpose of measuring the p-y response of a rigid wall supporting sand at different relative densities. The retaining system is 0.5 m wide, 1.2 m high, and 2.6 m long. A rigid side wall was designed to pivot about its bottom axis such that it can displace the soil in the active and passive directions. The method of pluviation was utilized for filling the system with dry sand to ensure a uniform density throughout the depth of the backfill. Dry sand backfills at three relative densities were tested under static lateral loading. Throughout testing, an effort was made to minimize side wall friction using grease and thin plastic sheets to mimic plane-strain conditions. The p-y curves were then determined using data from pressure sensors, load cells, and linear variable differential transformers (LVDTs).

SOIL RETAINING SYSTEM

The test tank consists of a 0.5 m wide, 1.25 m high, and 2.6 m long rectangular enclosure with an open top (fig. 1). The side walls are fabricated from 40 by 80 by 2.5 mm rectangular hollow sections welded to a 4 mm steel side plate. The side walls are braced against lateral bottom beams with side kickers at equal intervals. The bottom lateral beams are welded to the system's floor and thus constitute an integral part of the retaining wall system.

FIG. 1 Picture of the soil retaining system.

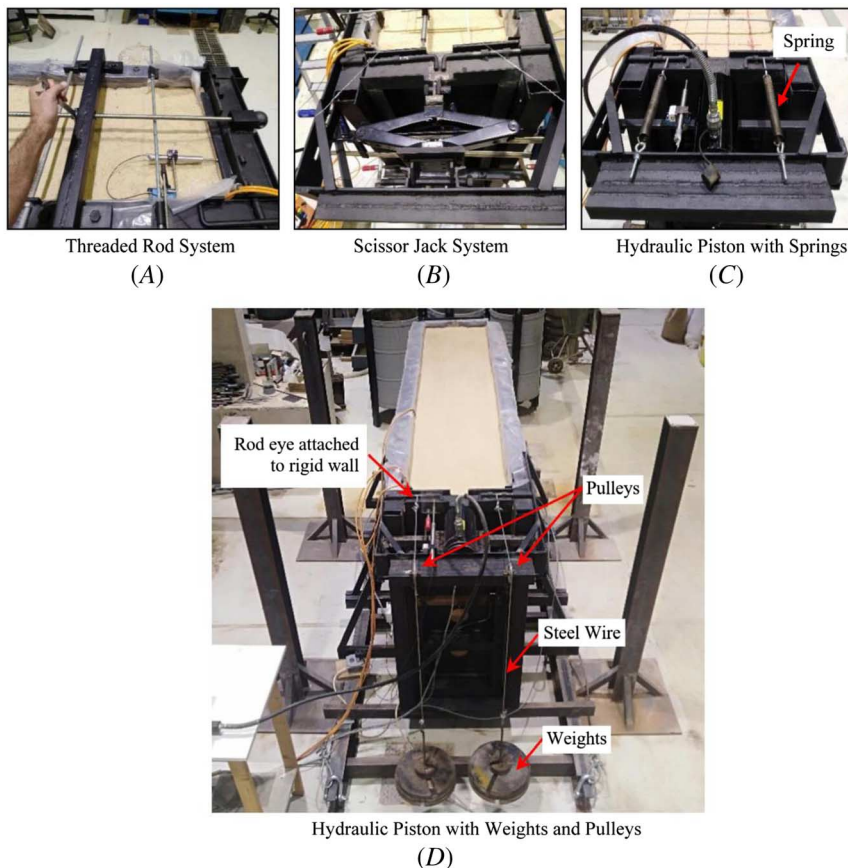


The front wall is stiffened by an H100 by 100 (I-beam) to withstand large lateral pressures while minimizing wall deformations. It is built with a hinging mechanism at its bottom and kept unrestrained at its top. Two manual locks are installed at the top of the wall to stabilize the wall during the setup phase. A similar design was adopted for the back wall, which was designed to flip open to facilitate access to the retaining system from the back side. The whole retaining system was designed as three separate blocks for ease of fabrication and possible relocation within the lab to be assembled with bolt systems at the side walls.

The length of the prototype was carefully chosen such that (1) it would be sufficient to allow for the passive failure wedge to develop within the retained sand and (2) no pressures will develop at the back wall that will cause unwarranted confinement pressure at the front wall. Once the wall dimensions were selected, a 3-D prototype was modeled on the structural analysis software SAP2000 to investigate the development of stresses and deformations on the side walls. Based on the structural analysis, the wall was designed to limit the side wall deformations to a maximum lateral deflection of 1 mm both during filling and upon the mobilization of passive conditions. A 1 mm lateral deflection was considered sufficient to simulate plane-strain conditions along the side walls.

The soil retaining system is designed to be a stand-alone unit capable of conducting an experiment unaided by a strong wall or an external loading frame. For this to be accomplished, a U-shaped bracket attached to the side walls capable of seating a lateral jacking system (fig. 2B) was used. Three methods were investigated for displacing the top of the wall: (1) threaded rod method, (2) scissor jack method, and (3) hand-driven hydraulic piston method. In the first case, moving the wall required a lot of man power and was therefore abandoned.

FIG. 2 Methods for displacing top of wall using (A) threaded rod, (B) scissor jack, (C) handheld hydraulic piston, and (D) hydraulic piston with pulleys.



In the case of a scissor jack, the jack buckled under the large passive pressure. The hydraulic pump and piston method was relatively easy to use allowing an adequate level of displacement control.

The displacing mechanism (hydraulic jack) was attached to the retaining system using a U-shaped bracket that utilized the sidewalls of the retaining system to create a stand-alone setup. The two springs shown in [figure 2C](#) were installed to eliminate gap formation between the wall and the hydraulic piston during active wall displacement. However, after a few trial experiments, it was found that the springs had to be extended significantly and were susceptible to permanent deformation. As a result, the spring system was replaced by weights extended around a pulley system and attached to the rigid wall (see [fig. 2D](#)).

One of the challenges in conducting laboratory experiments on retaining wall prototypes is the development of unfavorable friction forces along the inner sidewalls. These friction forces can unjustifiably increase or decrease lateral earth pressures measured on the moving wall. The interface friction angle between the backfill and the side walls varies with the roughness of the interface, the particle size, and the morphology of the sand.

Several methods are presented in the literature that aim at minimizing frictional stresses at the interface between soil and other materials ([Tatsuoka and Haibara 1985](#); [Fang et al. 2003](#)). These studies show that shearing soil against an acrylic plate while separating both materials by grease or thin layers of plastic sheets yields low interface friction angles. Silicon grease is used at the soil-acrylic plate boundary to reduce the interface friction angle. To keep the soil clean, a thin latex sheet is used to separate the soil from the grease. This method yields interface friction angles that are inversely related to the applied confinement pressures. At confinement pressures exceeding 10 kN/m^2 , the interface friction angle could be as low as 3° ([Fang et al. 2003](#)). Another method uses different layering sequences of thick and thin plastic sheets over an acrylic plate to reduce the interface friction. Although the latter can be quicker, more economical, and cleaner than the grease method, it yields higher interface friction angles reaching values between 10° and 15° for most plastic sheet sequences. As a result, the grease method was adopted for the setup developed for this study. The method that was adopted for its ease of application and efficacy entails creating a multilayered interface comprising of a thin plastic sheet, grease, and a thin plexiglass plate. Accordingly, a 4 mm plexiglass plate was attached to the sidewalls ([fig. 3A](#)). A thin layer of grease was smeared over the plexiglass using a spatula and a thin plastic sheet was laid over the grease ([fig. 3B](#) and [3C](#)).

Although this technique was proven to greatly decrease the interface friction angle, residual frictional forces will remain. To measure these forces, a special device was custom fabricated and attached to one of the sidewalls ([fig. 4A](#)). The device consisted of a low range force gage connected in parallel with a sliding block. The block was fitted in a rectangular cut made in the wall and placed flush with the interior surface ([fig. 4B](#)). The force gage is mounted to the outside wall to record the frictional forces. On the opposite wall and at the same elevation, another

FIG. 3 Reducing side walls friction. (A) Plexiglass on side walls, (B) grease application over plexiglass, (C) thin plastic sheet above grease.

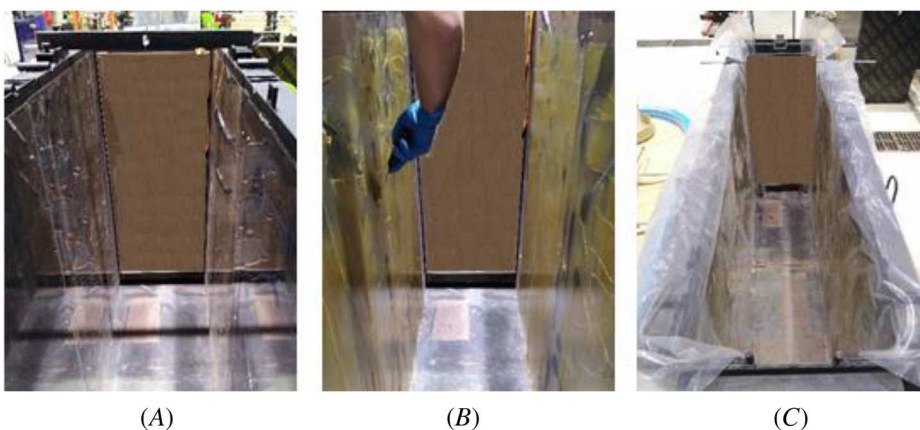
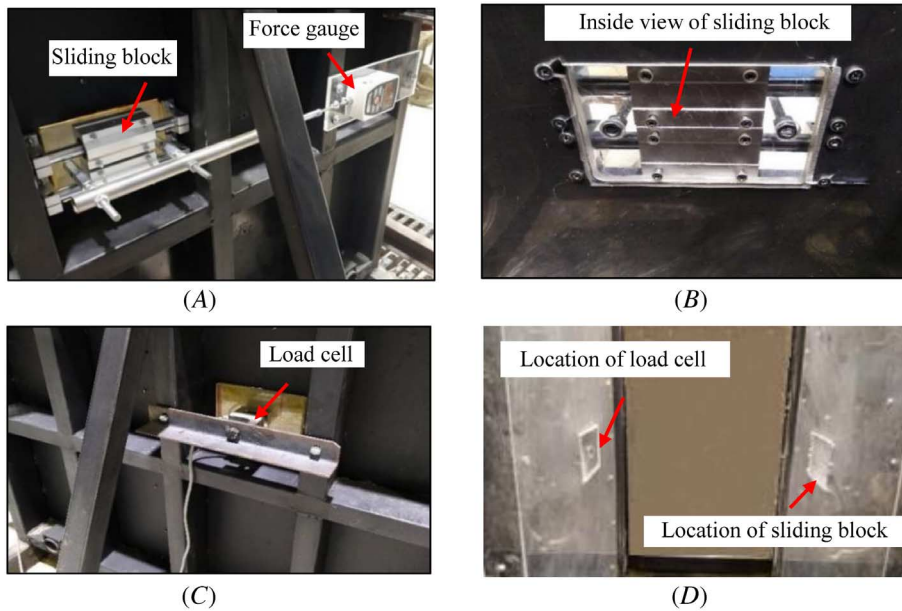


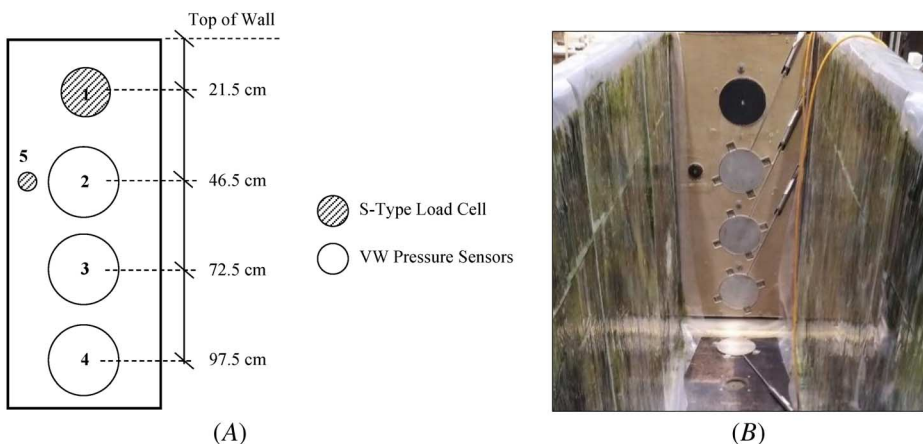
FIG. 4 Interface friction angle measurement: (A) parallel force gage and sliding block, (B) interior surface of sliding block flush with wall, (C) perpendicular load cell and fixed block, (D) interior sidewalls showing both gauges opposite to each other.



force gage was connected perpendicular to a fixed block in the same manner (fig. 4C) to measure the normal stress on the side of the wall. The frictional shear stress measured by the friction sensor was then divided by the normal stress measured by the pressure sensor to calculate the friction coefficient and interface friction angle for the side wall interface.

Three vibrating wire pressure sensors (fig. 5) and two S-type load cells were used for measuring the soil lateral pressure. The location of the sensors on the front wall is shown in figure 5A. The vibrating wire sensors (#2, #3, #4) have a diameter of 230 mm, whereas the S-type load cells (#1, #5) were attached to round plates having

FIG. 5 (A) Sensor location from the top of the wall; (B) pressure sensors installed in wooden board carved to fit sensors on front wall.



diameters of 160 and 60 mm, respectively. The vibrating wire sensors (VW) had a range of 0 to 350 kPa, a resolution of 0.025 % F.S. (F.S. being full scale), and an accuracy of ± 0.1 % F.S. The S-type load cells at 21.5 cm and 46.5 cm depth had load ranges of 0 to 500 lbf (2.2 kN) and 250 lbf (1.1 kN), respectively, with a resolution of ± 0.02 % FSO (Full scale output) and a repeatability of ± 0.01 % FSO. The calibration factors for the VW sensors were checked in-house using a calibration chamber that was custom fabricated in the form of a sealed water container that is subjected to an incremental increase in water pressure. The pressurized container is composed of a polyvinyl chloride (PVC) pipe (30 cm in diameter and 50 cm in length), two thick 40 cm by 40 cm by 10 mm steel plates overlain with a neoprene pad on one side, four threaded rods, and two one-way valves. The pipe is fitted between two steel plates with the neoprene pads facing the pipe ends. The threaded rods are used to squeeze the two plates to the pipe ends ensuring a water seal. Two valves are installed onto the top plate. One valve is used to deair the container, whereas the other is used as the pressurized water inlet.

The sensors were installed flush with the inside surface of the wall. To this end, the shapes of the pressure sensors were carved out of a 40 mm dense wooden board to fit the sensors flush with the surface of the board (fig. 5B). The wooden board was then attached to the front wall. To reduce the friction between the soil and the wooden board, a plexiglass plate was added onto the surface of the board. In addition, an extra pressure sensor was placed at the base of the retaining system to measure changes in vertical pressure while filling the tank and during the experiments (fig. 5B). Two LVDTs were placed on the front wall to measure the displacement at the top and mid-height of the wall. The rigidity of the wall was confirmed through the ratio of the displacements measured by the two LVDTs.

PLACEMENT OF BACKFILL

In this study, pluviation was used to ensure a uniform density for the sand in the backfill given the relatively large scale of the experiment (Dave and Dasaka 2012; Tabaroei, Abrishami, and Hosseininia 2017). The pluviation technique consists of “raining” sand down from a height (*HF*) at a constant discharge rate and deposition intensity to reach a preset density. Several pluviators of different complexities have been proposed in the literature. Portable pluviators generally include a sand storage compartment, a flexible delivery tube, an orifice that discharges sand at a given rate, a rigid tube of different heights to control the height of fall, and a sieve diffuser that is placed at the end of the rigid tube to rain sand in a uniform manner over a certain area.

A handheld portable pluviator was crafted for the present study (fig. 6) to be carried and moved by a crane and adjusted by hand. A steel barrel was used as a sand storage unit. A hole was cut at the bottom of the barrel to allow for sand to escape. A butterfly shutter was used to open and close that hole. The butterfly shutter was attached to a flexible tube to transfer the sand from the sand storage unit to the rigid tube where the sand is discharged. The rate of sand discharge was controlled by an orifice placed at the top end of the tube (fig. 6C). The flexible tube could be customarily tugged in different directions during the filling process, creating an inclination in the rigid tube. This inclination will pull the sand to one edge of the rigid tube and change the discharge rate and resulting density. To ensure a vertical position of the rigid tube, a leveling mechanism was fabricated and placed between the flexible and the rigid tube (fig. 6B). The leveling mechanism consists of four PVC reducers each with two consecutive reducers joined by a 6 mm rod that serves as a pivoting axis, allowing one reducer to twist while the second maintains its vertical position (fig. 6C). If only two reducers and one axis of rotation are present, then shifting the flexible tube along a line that is perpendicular to the axis of rotation keeps the rigid tube vertical. Movement in any direction twists the bottom reducer as well. Having four reducers joined with rods at 45° from each other gives the freedom for shifting the flexible tube in four directions while maintaining the last reducer vertical.

The height of the sand drop and the size of the orifice needed to produce a target density was determined by conducting pluviation tests using a cylindrical mold of known volume (fig. 7). Various orifice diameters, number of orifices, and associated pluviation heights were explored through calibration tests. Orifices with diameters of 6, 10, and 15 mm with 5 openings each were investigated. For each orifice size, the height of fall was varied and the density of the resulting sample was measured (fig. 7B). The results of the pluviation tests served as the basis for selecting the height of fall and the size of the orifice to achieve target densities of 1,550, 1,650, and 1,750 kg/m³.

FIG. 6 (A) Portable pluviator, (B) leveling mechanism, and (C) sieve diffusers and orifice.

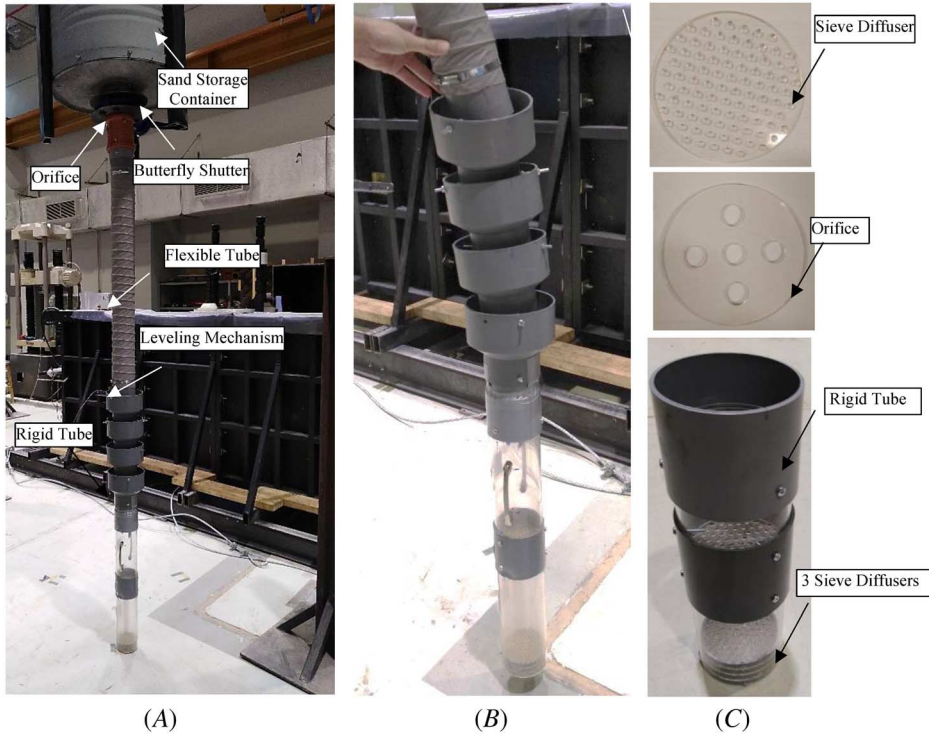
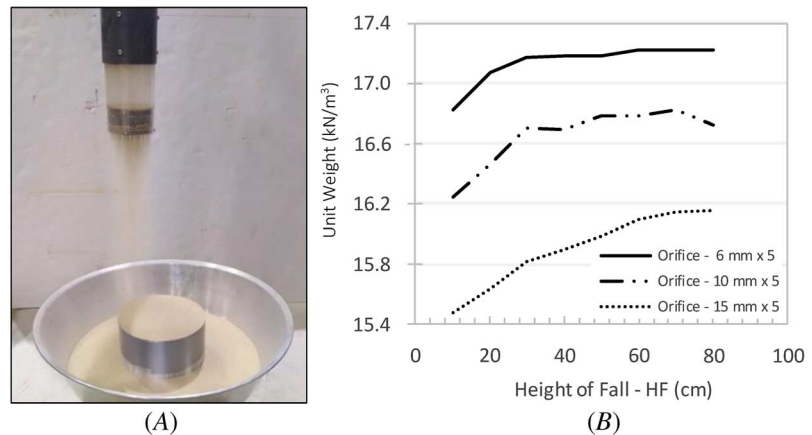


FIG. 7

(A) Pluviation conducted on small mold; (B) results of pluviation experiments.



The height of the fall and the size of the orifice used to control the flow rate for each soil density are summarized in **Table 2**. Trial pluviation tests were conducted on a miniature wooden box ($10 \text{ by } 40 \text{ by } 60 \text{ cm}^3$) to ensure that the target density can be reached. The traveling hopper was filled with sand and weighed before and after raining sand to determine the weight of soil dropped. The results of the trial tests indicated that the pluviation technique yields actual densities that are close to the target densities (**Table 2**).

Figure 8 shows the process of pluviation used to fill the soil retaining system. The first check on the achieved density was the record of the weight of the total soil placed into the tank divided by the volume. The second check

TABLE 2

The pluviation setup used to achieve the desired target densities

Target Density, kg/m ³	Actual Density, kg/m ³	Height of the Fall, cm	# of Openings × Diameter of Orifice	Flow Rate, kg/min/cm ²
1,550	1,547	10	5 × 15 mm	0.481
1,650	1,668	35	5 × 10 mm	0.145
1,750	1,748	60	5 × 8 mm	0.033

FIG. 8 Filling the soil retaining system with sand using pluviation.

was done through the density achieved in a small mold that was placed on the floor of the tank prior to pluviation. Upon the completion of testing and emptying of the tank, the small mold was retrieved and the density checked.

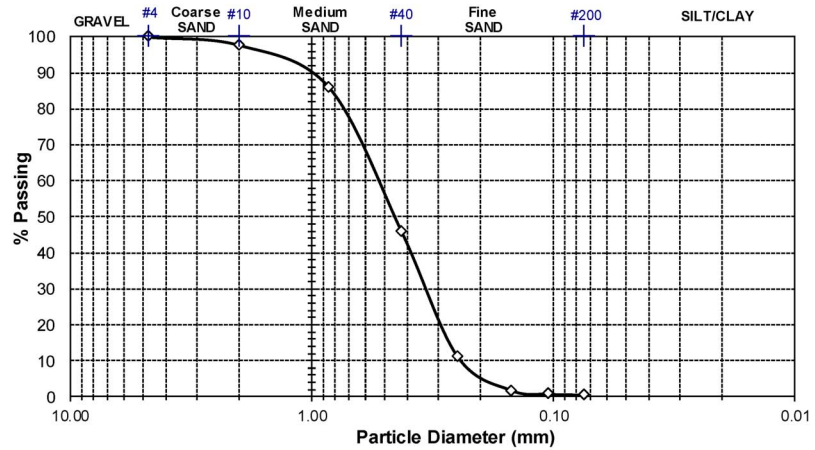
SOIL CHARACTERIZATION

The index properties of the sand were determined from sieve analysis (ASTM D6913, *Standard Test Methods for Particle-Size Distribution (Gradation) of Soils Using Sieve Analysis*), specific gravity (ASTM D854, *Standard Test Methods for Specific Gravity of Soil Solids by Water Pycnometer*), and maximum and minimum dry density tests (ASTM D4253, *Standard Test Methods for Maximum Index Density and Unit Weight of Soils Using a Vibratory Table*, and ASTM D4254, *Standard Test Methods for Minimum Index Density and Unit Weight of Soils and Calculation of Relative Density*). The grain size distribution curve indicates that the sand is composed of 99.5 % sand and 0.5 % fines (fig. 9). The coefficient of curvature $C_c \left(= \frac{D_{30}}{D_{60}D_{10}} \right)$ and the coefficient of uniformity $C_u \left(= \frac{D_{60}}{D_{10}} \right)$ were calculated to be 1.2 and 0.68, respectively. According to the Unified Soil Classification System, the soil is a poorly graded clean sand with little or no fines, SP. The average specific gravity from three tests was calculated as 2.64. The minimum and maximum void ratios were found to be 0.47 and 0.81, respectively.

Given that the experimental setup involves a relatively short wall (1.2 m height), the initial confining stresses in the sand bed at the location of the sensors are expected to be in the low pressure range (5 to 20 kPa). Consequently, the Mohr-Coulomb failure envelope that characterizes the shear strength of the sand in the bed is expected to be curved. Isotopically consolidated drained triaxial tests (ASTM D7181-20, *Standard Test Method for Consolidated Drained Triaxial Compression Test for Soils*) were conducted on

FIG. 9

Grain size distribution for the backfill sand.



dry sand specimens under confining pressures of 10, 20, and 50 kPa to determine the friction angle of the sand at relatively low confining pressures. Sand specimens with a diameter of 7.1 cm and a length of 14.2 cm were prepared at three densities (1,550, 1,650, and 1,750 kg/m³) to mimic the densities used in the sand bed experiments. All sand specimens were sheared under static loading conditions at a typical strain rate of 1 % per minute.

The variations of the deviatoric stress and the volumetric strain with axial strain are presented in **figure 10**. As expected, the loose sand specimen exhibited a contractive volumetric response that resulted in a strain hardening. Conversely, the medium dense and dense specimens presented a dilative response with clear peaks at strains of about 5 to 10 %. The densest specimen exhibited the largest deviatoric stress and volumetric strain at failure (~7 %).

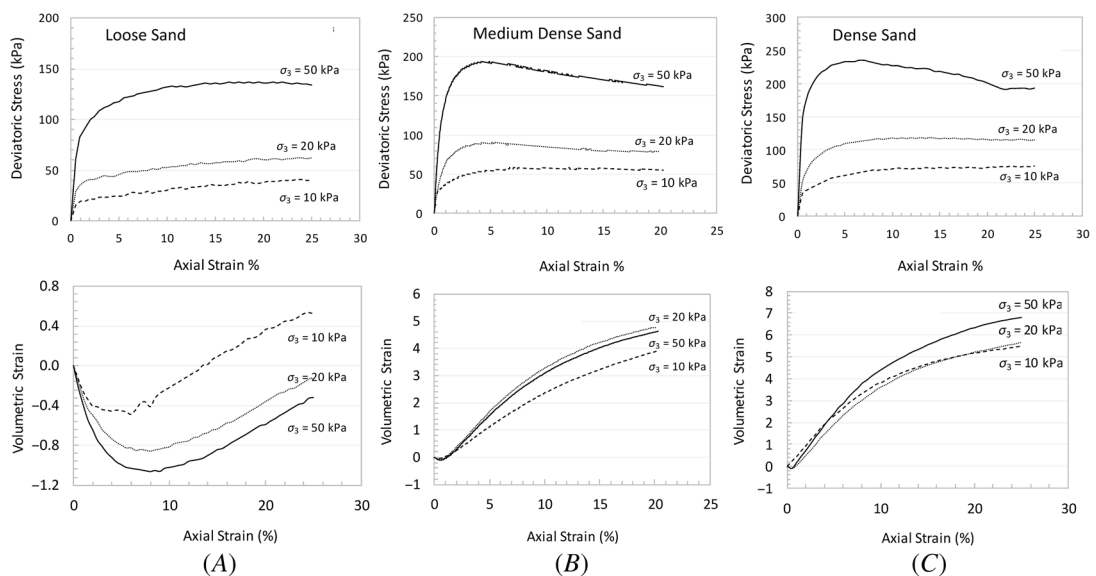
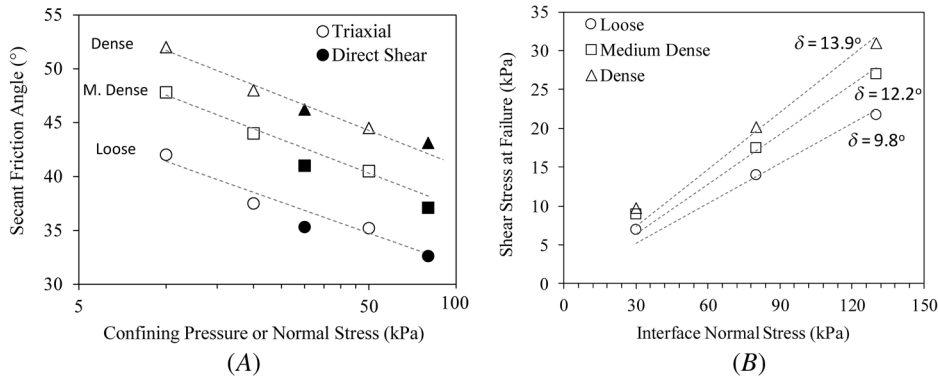
FIG. 10 Variation of deviatoric stress and volumetric strain with axial strain for consolidated drained tests on (A) loose, (B) medium dense, and (C) dense sand specimens.

FIG. 11 (A) Secant friction angle of the sand and (B) Interface friction angle between the sand and acrylic for loose, medium-dense, and dense sand from triaxial and direct shear tests.



The drained secant friction angle of the sand was determined at each confining stress and sand density. The friction angles show a clear decreasing trend with the logarithm of confining pressure (fig. 11A). For loose sand, the friction angle decreases from 42° to 35° as the confining pressure increases from 10 to 50 kPa. Higher friction angles were obtained for medium dense and dense sands in which the friction angle decreases from 47.5° to 40° and from 52° to 44°, as the pressure increases from 10 to 50 kPa. The rate of decrease of the secant friction angle with the logarithm of the confining pressure was remarkably similar in all tests. These results confirm the curvature of the Mohr-Coulomb envelope in the low pressure range, indicating that the friction angle of the sand in the bed is expected to vary with depth, with expected differences of about 5° between the location of Sensor #1 (confining pressure less than 5 kPa) and Sensor #4 (confining pressure between 15 and 20 kPa).

To confirm these results, two additional static direct shear tests were conducted on 60 by 60 by 10 mm dry sand specimens at normal stresses of 30 and 80 kPa. The samples were sheared at a displacement rate of 1 mm per minute. The resulting secant friction angles are clearly in line with the triaxial test results as observed in figure 11A.

SAND/WALL INTERFACE STRENGTH

The interface friction angle between the sand and the moving/rotating wall has a significant impact on the lateral earth pressure mobilized at the wall. For the experimental setup adopted in this study, the backfill sand will slide against a 4 mm acrylic plate mounted on the front wall. The acrylic plate was used on the front wall in order to reduce interface friction. It is imperative, therefore, to quantify the interface friction angle of sand against acrylic.

The determination of the interface friction angle of sand on acrylic was done using static interface direct shear tests at sand densities of 1,550, 1,650, and 1,750 kg/m³. An acrylic plate was fitted tightly in the lower shear box and sand was placed in the upper half of the shear box at the desired density. The Mohr-Coulomb failure envelopes that were fitted to the interface direct shear data for the three relative densities are presented in figure 11B. Results indicate that the interface friction angle between the sand and acrylic ranged from 9.8° to 13.9°. The lower friction angles represent conditions in which the sand was at the smallest relative density, whereas the higher friction angle corresponded to tests at the highest relative density.

Experimentally Derived p-y Curves

In this section, experimentally derived active and passive p-y relationships are determined for sand beds with three relative densities to quantify the effect of relative density on the static p-y response. The tests involved full

static cycles of loading, with each cycle initiating by displacing the wall from its at-rest condition to an active condition, followed by passive loading up to a maximum wall displacement of 10 % of the height of the wall (around 120 mm). Two additional cycles that involved unloading the wall from passive to active and from active to passive were then enforced. The goal of these cycles was to quantify the changes to the p-y response if the wall is subjected to large displacement cycles.

TESTING PROCEDURE

A hand-operated displacement-controlled hydraulic piston capable of moving in increments of 0.01 mm was used to displace the top of the wall. In order to limit the development of frictional sidewall forces, the speed of the top-wall movement had to be carefully monitored. Displacing the wall at a fast rate can result in an increase in the frictional forces at the side walls because of the viscosity of the grease layer. To minimize frictional forces on the side walls, a slow rate of wall movement was enforced by pumping the hydraulic piston using small strokes. In addition, the wall movement was stopped (2–10 min) after each increment of wall displacement for the system to release/dissipate any built-up frictional stresses at the sidewalls.

The experimental program involved subjecting the top of the wall to two successive phases of wall displacements. Phase #1 consisted of displacing the top wall from the at-rest position to –8 mm in the active direction, [0, –8 mm], whereas Phase #2 consisted of displacing the top wall from the –8 to 120 mm in the passive direction, [–8, 120 mm]. The –8 mm top-wall displacement in Phase #1 is considered (1) large enough to determine the active p-y curves and (2) small enough to not influence the passive soil behavior in Phase #2.

It should be noted that the choice of a pure “rotation” wall movement in the experimental program mimics the expected response of rigid basement walls for buildings subject to cyclic loading. Previous numerical studies (El Ganainy and El Naggar 2009; Saad, Najjar, and Saddik 2016) indicate that under cyclic loading conditions, the deformation of the basement walls for such buildings is generally governed by an overall net rotation that results from the difference between the translation at the base and top of the wall (translation at the base is generally in the order of 10 to 20 % of the translation at the top of the wall). Numerical solutions also show that the lateral stress versus displacement relationship (p-y relationship) behind a rigid wall is not sensitive to the translation of the wall at the tip (Elchiti et al. 2017; El-Chiti et al. 2018). As such, we opted to adopt a pure rotation of the wall by only displacing the wall at the top. This simplifies the experimental setup needed to measure the p-y response without compromising the resulting p-y curves.

RESULTS AND DISCUSSION

Medium Dense Sand

The p-y curves constructed from the data collected at the four sensors for the case of a medium dense sand backfill ($\rho = 1,650 \text{ kg/m}^3$) are shown in figures 12 and 13 for the at-rest-to-active and active-to-passive responses, respectively. The at-rest and limit-state Coulomb stresses are denoted in the figure by the green and red hatched lines, respectively.

A number of observations can be made based on the shape of the at-rest to active p-y curves. Except for the p-y response of Sensor #1, active p-y curves are characterized by monotonic decreases in stress from the at-rest to limit-state active condition. The curves are nonlinear with an observed decrease in the rate of stress reduction with increased wall displacement. On the other hand, Sensor #1 measured a constant stress that is almost close to the active limit-state stress even before displacing the wall. The proximity of Sensor #1 to the hydraulic piston at the top of the wall renders it sensitive to any accidental movement during the preparation process, possibly resulting in premature mobilization of active stresses. Figure 12 clearly shows that the lateral earth pressures are highly sensitive to active wall displacement. A top wall displacement of –8 mm was sufficient to drop the lateral pressures from the at-rest pressure to active limit-state pressure at all sensors. In fact, local displacements as low as 2 mm could be considered sufficient to mobilize the active limit state in the majority of the sensors.

FIG. 12 Static active p-y curve for medium-dense backfill ($1,650 \text{ kg/m}^3$). A.P. indicates active pressure.

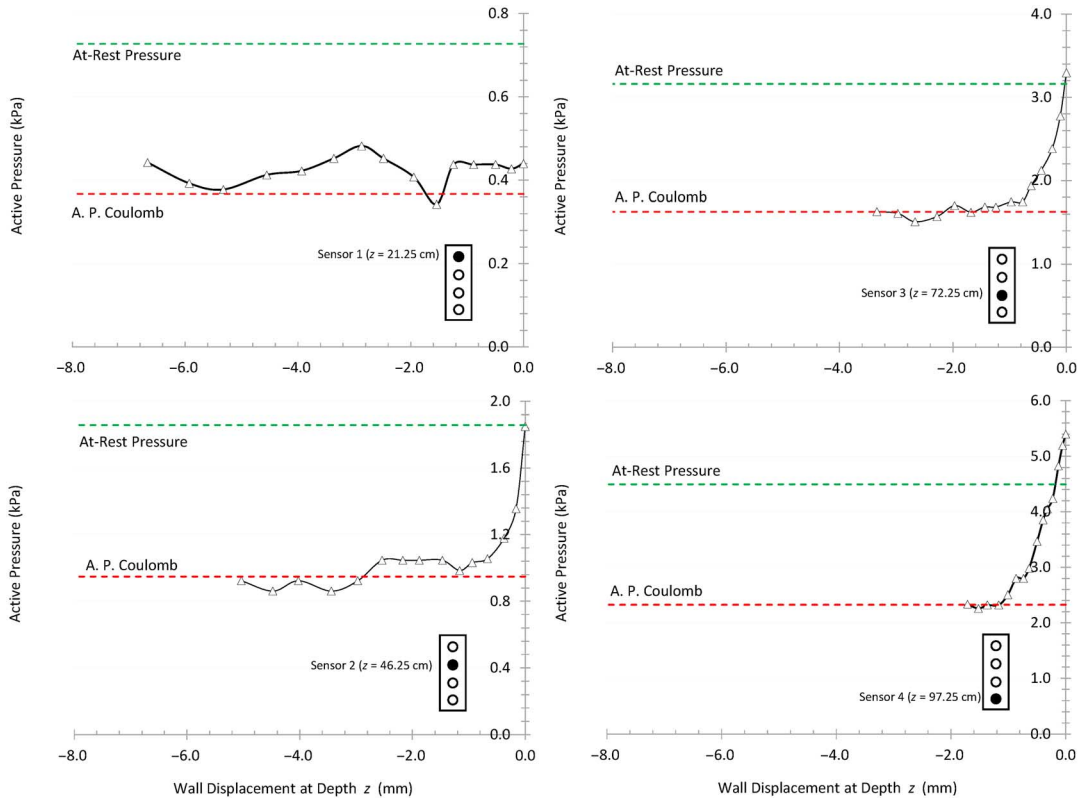


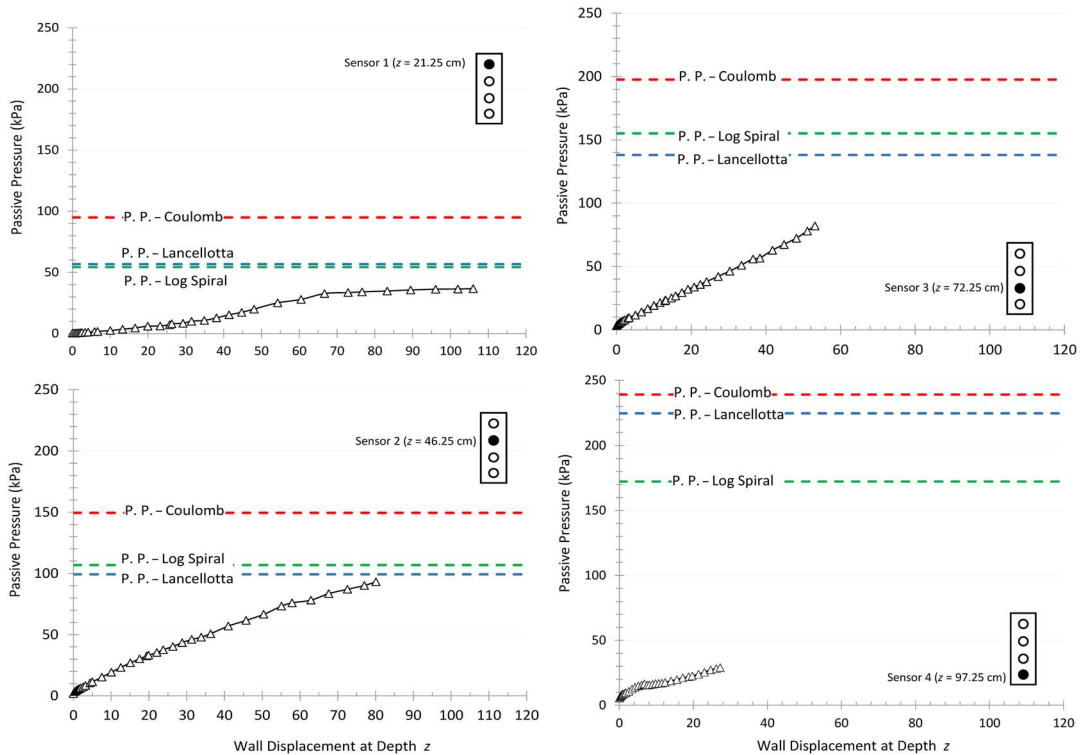
Figure 13 shows the variation of the lateral stresses with wall displacement as the wall was pushed from the active side to the passive side. To put the measured passive p-y response in perspective, different limit-state pressures based on renowned theories are superimposed in **figure 13**. These include passive pressure theories from Coulomb (1776), Lancellotta (2002), and Liu et al. (2018), the latter being based on the assumption of a log-spiral slip surface. The theoretical passive pressures were determined from the soil and interface properties, ϕ and δ , that were extracted from the data presented in **figure 11**.

The measured at-rest to passive p-y response is characterized by a monotonic increase in lateral pressure with inward wall displacement. The response is nonlinear with varying intensity depending on the location/depth of the sensor and the magnitude of the applied displacement. The p-y response at Sensor #1 is S-shaped, a characteristic of relatively unconfined sand. The p-y responses at Sensors #2, #3, and #4 have a slight negative curvature that would be more visible if higher pressures were reached.

Among the four sensors, only Sensor #1 traveled enough distance (wall displacement of 100 mm) for the mobilized stresses to stabilize at limit state. On the other hand, the mobilized stresses at Sensors #2, #3, and #4 increased either at the same rate or with a slightly reduced rate showing no signs of asymptotic behavior. This is due to the relatively small wall displacements that were applied at these sensor locations. The small displacements were not large enough to induce nonlinearity in the passive p-y response. As a result, passive limit state was not reached in the lower sensors. The reduction in the enforced wall deformations at the locations of the deeper sensors is attributed to the pure rotational movement of the wall whereby Sensor #1 travels the most and Sensor #4 the least.

It should be noted that moving the wall into the active state and then conducting the passive cycle might slightly affect the passive response in the very early stages of loading. This is why the wall displacement at the

FIG. 13 Static passive p-y curve for medium-dense backfill ($1,650 \text{ kg/m}^3$). P.P. indicates passive pressure.



location of most sensors was restricted to less than 5 mm in the active cycle. Given that the “active” failure wedge behind the wall has a steeper inclination in comparison with the “passive” failure wedge, it is likely that the relatively small wall displacement in the “active” direction (which is restricted to the active soil wedge) did not affect in any appreciable way the main response in the “passive” soil wedge. It might have affected the slope of the p-y curve in the first couple of millimeters of wall movement; however, it would not have any marked effect on the response at larger displacements.

The active and passive p-y curves for the medium dense sand are presented in [figure 14](#) for comparison. As shown in the figure, the rate of stress decrease in the case of active wall displacement shows little dependency on the depth of the sensor. However, care should be taken before generalizing such behavior to full scale walls, given that the experiments are conducted on a soil depth that is generally shallow (120 cm). For the case of the passive response, with the exception of Sensor #1, the three lower sensors showed a relatively similar initial stiffness in the p-y response. The stiffness at the location of Sensor #1 was somewhat smaller because of the relatively low confinement level. However, only the p-y response at Sensor #1 exhibited a full mobilization of passive conditions at local wall displacements ranging from 80 to 100 mm.

[Figure 15](#) shows the lateral stress distribution along the wall height at top wall displacements of 30, 60, 90, and 120 mm. Results indicate that the maximum stress was recorded at Sensor #2 or at approximately 1/3 of the wall height. The shape of the resulting stress distribution with depth is attributed to the coupled effect of the variation in the confinement stress ($\gamma \cdot z$) with depth and the local displacement of the wall at that given depth (y). It is known that lateral passive stress increases with both confinement and wall displacement. In the case of a rigid wall pivoting about its bottom axis, larger depths of confinement are accompanied with smaller wall displacements. When the latter outweighs the former, a decrease in lateral stress is registered, as was the case in Sensors #3 and #4.

FIG. 14 (A) Active p-y curves for medium dense soil for all sensors and (B) passive p-y curves for medium dense soil for all sensors.

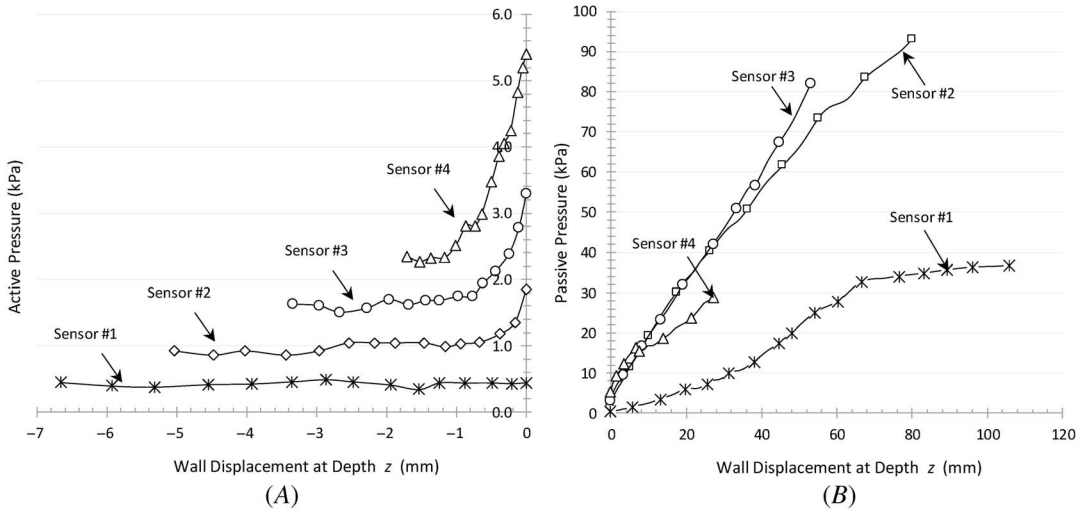
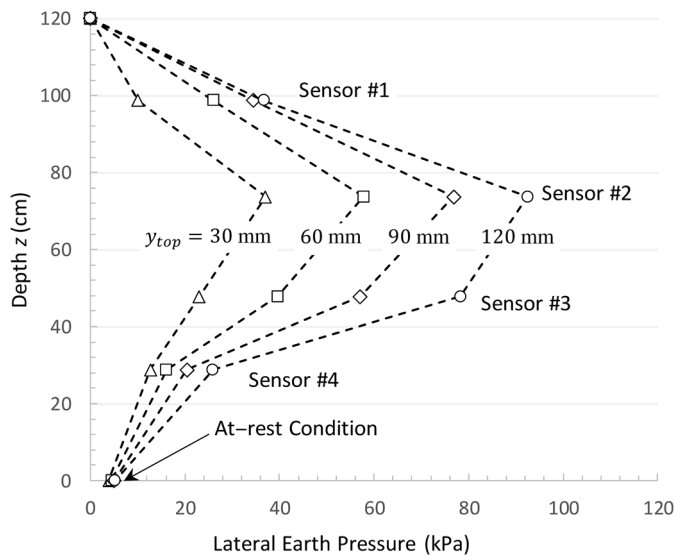


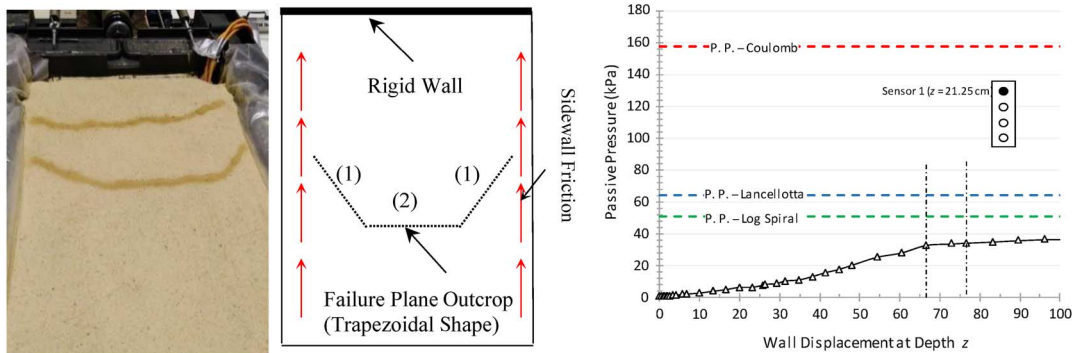
FIG. 15

Variation of the lateral passive stress with depth in the sand bed.



Displacing the wall in the passive direction resulted in surface heave up to a maximum distance of 70 cm from the face of the wall. At 80 mm of top wall displacement, one of the failure planes propagated to the surface (fig. 16A) at a distance of about 17.5 cm from the face of the wall. This was followed by another surface trace at a top wall displacement of 92.5 mm. The second failure plane was observed at a distance of about 30 cm from the face of the rotating wall. The failure planes were marked with darker soil to increase their visibility. The surface traces of both failure planes can be approximated as trapezoidal in shape with the two end segments pulled back toward the rigid wall (fig. 16B). The shape of the failure plane is probably affected by the friction on the side walls, which restrains the sand bed at the edges of the tank from displacing horizontally as the wall is forced to rotate.

FIG. 16 Surface traces of two failure planes forming in front of the wall in the medium-dense soil and their relationship to the p-y response at Sensor #1. P.P. indicates passive pressure.



The presence of a horizontal segment in the failure plane gives assurance that the central part of the failure plane seems to be unaffected by the boundary effects caused by side wall friction. Because all pressure sensors are located at the center of the rotating wall away from the side wall edges, it is expected that the pressure readings in the sensors were not affected by side wall friction, which was minimized to the smallest values possible using the alternating layers of plastic and grease.

Figure 16C shows the passive p-y response at Sensor #1 with the wall displacements at which the failure planes surfaced. The surface traces of the two failure planes were accompanied by significant reduction in the rate of stress increase as the p-y response shifts to an asymptotic response. It is expected that when a failure plane completes its trajectory toward the surface of the soil (i.e., becomes visible), constant shear stresses along the failure plane are formed. This explains the stable p-y response observed at Sensor #1. Meanwhile, no effect of failure-plane formation was observed on the p-y responses of Sensors #2, #3, and #4. The distance from the rigid wall to Failure Planes #1 and #2 were measured to be 17.5 and 30 cm, respectively. The proximity of the failure planes to the rotating wall implies that the two planes originated from shallow depths that are expected to fall between Sensors #1 and #2.

The interface friction angle at the side wall was calculated during passive wall displacement using the friction sensor and force sensor installed at the sidewalls. Figure 17 shows the mobilized interface friction angle calculated at every incremental step of top wall displacement. The first curve in the figure denotes the interface friction angle calculated at the beginning of every intermittent pause, whereas the second curve denotes the interface friction angle calculated at the end of the intermittent pause. The first reading provides information on the effect of rate of loading, whereas the second reading provides information on the residual frictional forces remaining within the system before the second incremental displacement is launched.

During the experiment, the first reading was closely monitored as the speed of activation of the hydraulic pump was continuously modified to keep the first reading as low as possible but within practical constraints. As noted earlier, the speed of activation of the hydraulic pump and the magnitude of the side friction walls are related to the viscosity of the grease layer placed between the polyethylene sheet and the acrylic plate. Figure 17 indicates that the maximum interface friction angles at the sidewalls when the lateral pressures were recorded did not exceed 4° . This is relatively low, validating the process adopted for reducing the side wall friction in the experimental setup.

Effect of Relative Density on p-y Response

The experiment conducted on medium dense soil was repeated for the cases of loose and dense sand. Active and passive p-y responses at Sensors #2 and #3 for the three densities are compared in figure 18. The at-rest to active

FIG. 17

Interface friction angle calculated at side wall.

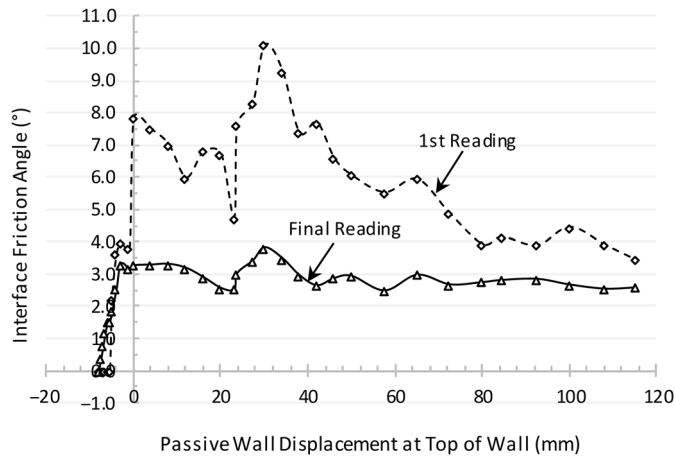
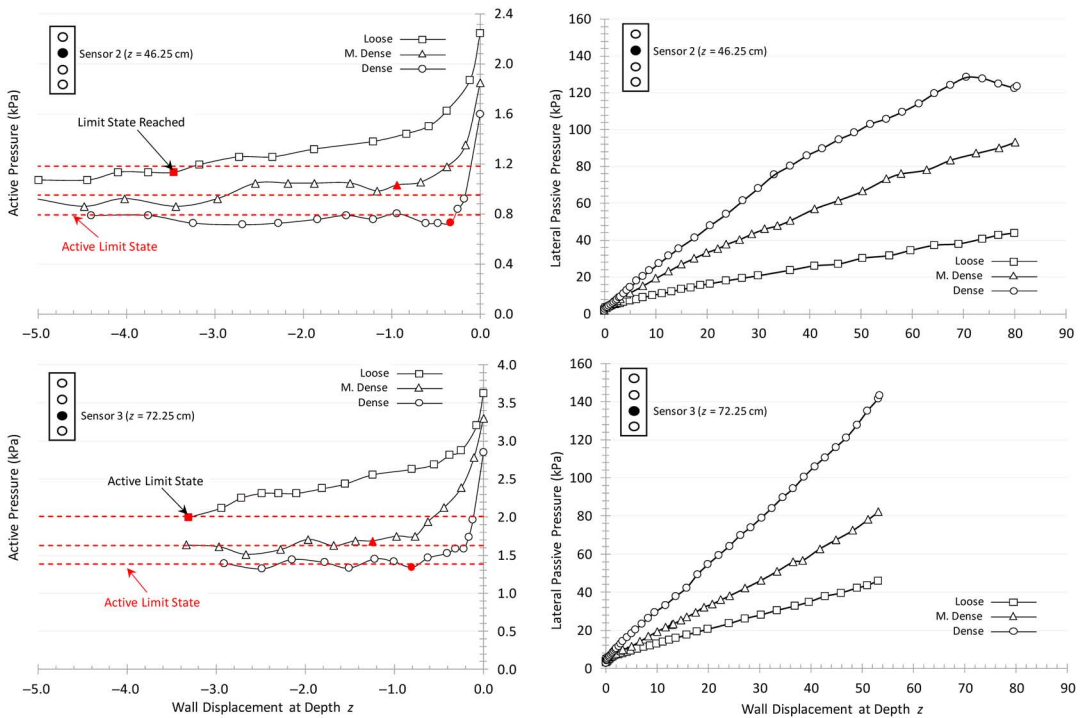


FIG. 18 Active and passive p-y response recorded at Sensors #2 and #3 for all densities.



p-y response of loose and dense sands was relatively similar to the response observed in the case of medium-dense soil. However, the rate at which active p-y curves approach their asymptotic active values varies with relative density. The solid red markers shown in figure 18 denote the wall displacement at which active limit state is reached. Loose sand was the slowest to approach the limit state followed by medium-dense and dense sand, respectively. The amount of wall displacement required to mobilize active conditions for the case of loose soil (3 to 4 mm) is approximately 3.5 times that for medium-dense soil and 8.0 times that of dense soil. Because the rate of

decrease in lateral pressure with active wall displacement is expected to be correlated to the stiffness of the backfill, it is expected that the active limit state for looser soils will require larger wall displacements in order for the lateral pressure at the wall to stabilize at active conditions.

Figure 18 shows the passive p-y response at Sensors #2 and #3 for the three soil densities. As expected, denser sand tends to exhibit stiffer p-y responses compared with looser sands. For all p-y responses, a monotonic increase in passive pressure is recorded except for the p-y response at Sensor #2 for the case of dense sand, in which softening was observed after the peak passive pressure was reached, a common characteristic of dense soil. Slight nonlinear behavior in passive p-y response is observed at relatively larger wall displacements, with less intensity in Sensor #3 because of the small wall movement recorded at that sensor.

Two failure planes daylighted at the surface during the passive displacement of the dense sand, whereas none were observed for the loose sand backfill. The first and second failure planes occurred at a top wall displacement of 100 mm ($\sim 8\%$ drift) and 110 mm ($\sim 10\%$ drift), respectively, as indicated in **figure 19**. The appearance of the failure planes at the surface was associated with the registration of a peak stress at Sensor #2. The fact that the recorded pressure at Sensor #3 was not affected by the formation of the failure plane indicates that the lower tip of the plane lies at or slightly above Sensor #2.

Both failure planes were nonplanar in shape with a concavity directed toward the wall. As in the case of medium-dense sand, nonplanar failure surfaces are indicative of the presence of residual sidewall frictional forces. The distances from the rigid wall to the crest/tip of the first and second failure surfaces were measured to be 36 and 81 cm, respectively. These distances from the rotating wall are greater than those observed during the test with medium-dense sand. This indicates that denser sands formed shallower passive failure wedges than looser sands. This falls in line with the general understanding of Rankine's theory in which the angle that the failure plane makes with the vertical depends on the friction angle of the sand (ϕ) and is calculated to be $45 + \phi/2$. Because denser soils have larger values of ϕ , it would be expected that denser soils result in less steep failure wedges.

Multiple Loading Cycles

In this section, the effect of "large-displacement" cycles of loading on the p-y response of retained loose medium-dense and dense sands is investigated. The term "large-displacement" is used in this section to differentiate these cycles from "smaller-displacement" repetitive cycles that could be investigated in future work to mimic seismic loading of the wall. At the end of the first loading cycle (active to passive), the pivoting rigid wall was oscillated three times between the two preset top wall displacements of -8 and $+120$ mm.

FIG. 19 (A) Formation of failure planes for the case of dense soil and (B) Wall displacement corresponding to the formation of failure planes.

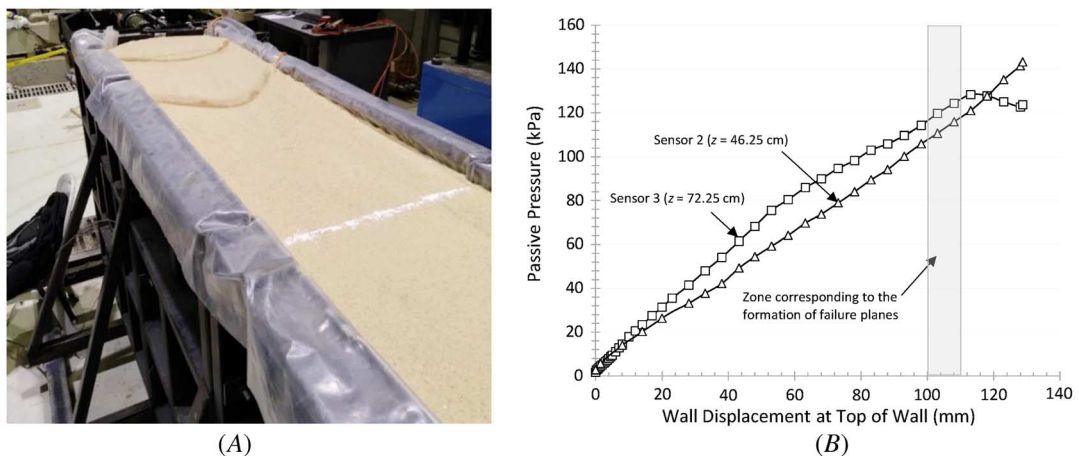


FIG. 20 The p-y response for medium-dense sand when subjected to three large cyclic loadings. P.P. indicates passive pressure.

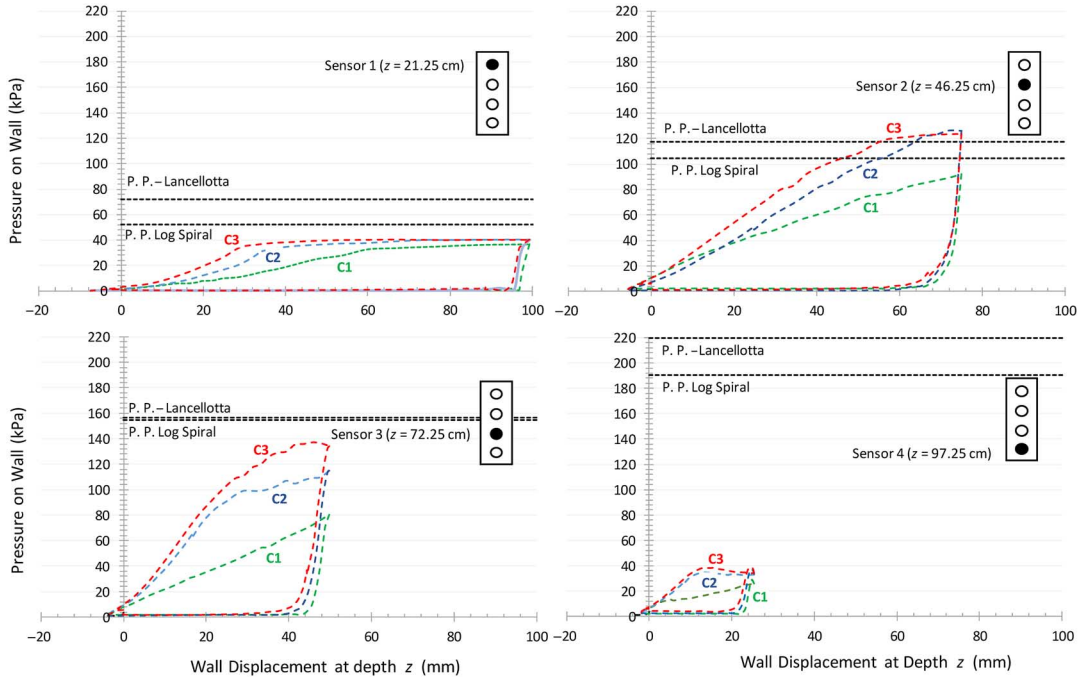
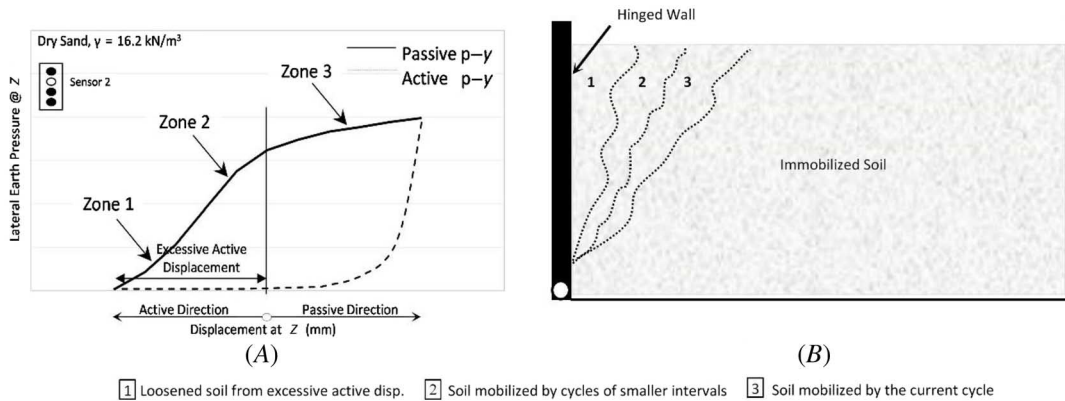


Figure 20 shows the p-y response for the medium-dense soil when subjected to three loading cycles. Several behavioral traits define the observed p-y response. The passive p-y response clearly shows that there is an increase in the passive soil resistance with each loading cycle. This is attributed to an increase in the sand density following passive loading. Large-displacement passive loading strains the sand in the failure wedge behind the moving wall and reduces the void ratio. Returning the wall back to its original position in the following active cycle will not revert the sand density back to the original value. As a result, successive densification of the backfill soil will occur after each loading cycle, leading to an increase in the peak stress with loading cycles. This holds true as long as the recorded peak stress does not reach the limit-state stress.

Results in figure 20 also indicate a change in the shape of the passive p-y curves with cycles of loading. This is observed by comparing the passive p-y responses of Cycles #1 with Cycles #2 and #3. The passive p-y response of Cycle #1 is mostly nonlinear with a negative concavity. However, in Cycles #2 and #3, the p-y responses take on an S-shape. The formation of “S-shaped” p-y curves in soil-structure-interaction problems has been observed by others (Yankelevsky, Eisenberger, and Adin 1989). A typical S-shaped curve is shown in figure 21.

Possible explanations for the formation of the “S-shaped” p-y response focus on the formation of three distinct zones of different soil densities just behind the moving wall (fig. 21B) as a result of cyclic movements. Zone #1 is a zone of loose soil formed by excess active wall movement in a previous unloading cycle. Excess active displacement denotes wall movement in the active direction beyond the displacement needed to mobilize the active limit state. Zone #1 contains soil of least density among the three zones. Zone #2 represents the soil affected by the loading/passive cycle of the previous interval and is expected to contain soil of the highest density among the three zones. Zone #3 represents soil that is being affected by the current interval displacement and contains a soil density equal to that of the undisturbed soil in the bed (initial density). As indicated in figure 21, the shape of each segment of the S-shaped curve can be attributed to straining soil in each of the aforementioned zones.

FIG. 21 (A) Typical p-y cycle; (B) formation of zones of different soil densities due to cyclic loading.



The data in [figure 20](#) clearly indicates that a large magnitude of top wall displacement is required for a passive limit state to be reached. Except for Sensor #1, which is located at a depth of 20 % of the wall height, none of the other sensors reached the limit state during the first cycle of passive displacement. Only after the densification of the soil had taken place did the soil reach its limit state. The measured passive stresses at large displacements were well-captured by the theoretical estimates of the passive stresses as predicted using the log-spiral method ([Liu, Xia, and Liang 2018](#)) and [Lancellotta \(2002\)](#)'s lower bound theory. Coulomb's theory, on the other hand, overestimated the passive limit state. It has been shown that Coulomb's theory overpredicts passive pressures for walls when $\delta > \phi/2$.

The term "preloaded active p-y curve" is used in this study to denote the part of the curve that extends from the peak passive stress to the lowest lateral stress recorded at $y = -8 \text{ mm}$. Several behavioral trends can be observed in [figure 20](#) in relation to the preloaded active p-y curves. First, the curves can be characterized as monotonically decreasing nonlinear curves with a shape that is dominated by a steep drop in lateral pressure recorded immediately after unloading from the passive state. The lateral stresses that build up during passive wall displacement are lost within the first few millimeters of active wall displacement ($\approx 5 \text{ mm}$). Second, the initial slope of the active p-y response is independent of the number of cycles the retained soil has been subjected to. At any given sensor, there is almost an identical response in the three preloaded active p-y curves. Third, the initial slope of the loading curve and the initial slope of the unloading slope are significantly different with the latter being much steeper than the former. The unload-reload behavior of any prediction model that aims at incorporating the unloading portion of a previously loaded wall should reflect this observation. Finally, the shape of the active p-y curves originating from at-rest conditions differs significantly from the preloaded p-y curves. As such, a unified model for static and cyclic loading should be avoided when modeling active p-y curves for rigid wall supporting sand.

In addition to the two failure planes presented in [figure 16](#) for the medium dense sand case, a new failure plane surfaced during the third cycle ([fig. 22](#)). What distinguished the third failure plane from the rest is the distance from the face of the rotating wall at which it surfaced. The first two failure planes formed close to the rotating wall, whereas the third one formed at an approximate distance of 150 cm ($\approx 60 \%$ of the length of the bed). To assess the depth of the failure wedge, the p-y response for the third cycle was investigated at all sensor locations. Results indicate that all four sensors reached limit-state passive pressures when the failure plane was observed. This is indicative of the depth of the failure plane, which seems to have extended beyond the first three sensors.

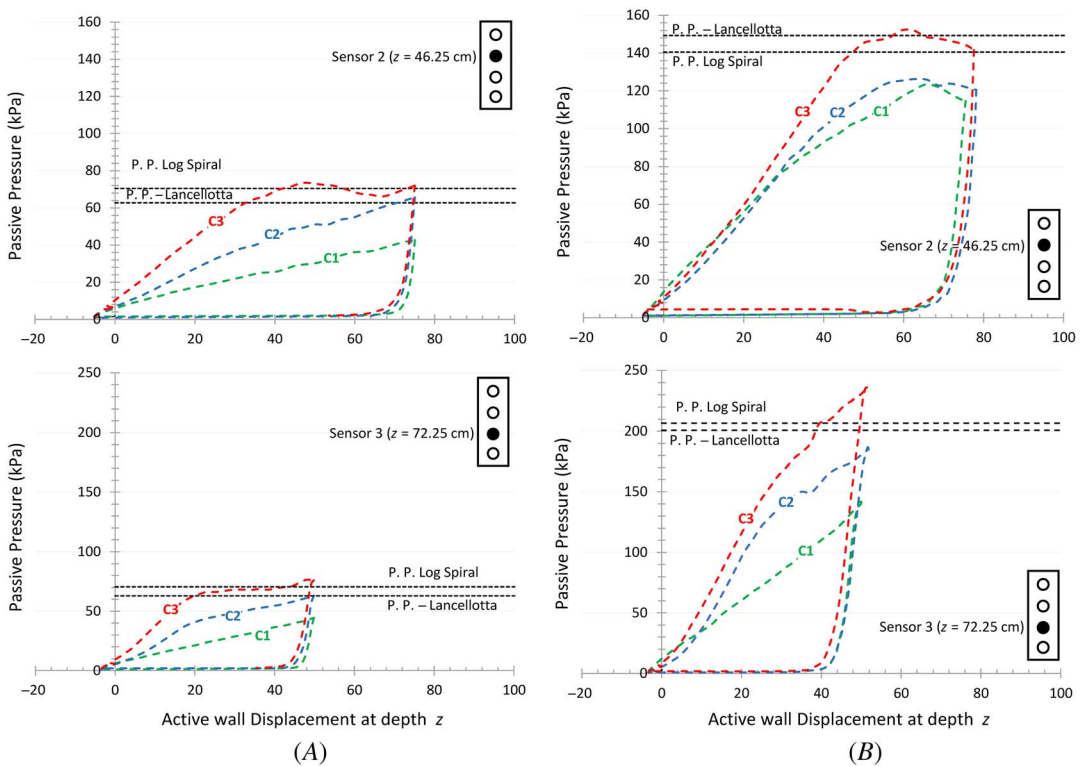
The p-y responses for loose and dense sand caused by large cyclic loading are shown in [figure 23](#) for Sensors #2 and #3. For the case of loose soil, three cycles were required for Sensor #2 to reach the limit-state stresses, whereas the limit-state stresses were noticed in the first cycle for the case of dense soil. Second, densification of

FIG. 22

Formation of a third failure plane in response to three cyclic loading (medium sand).



FIG. 23 The p-y response for (A) loose soil and (B) dense soil due to three cyclic loadings. P.P. indicates passive pressure.



sand by large cyclic loading is more pronounced in loose soil. The increase in lateral stresses between two successive cycles at any wall displacement is more significant in the case of loose soil. Finally, the small error between the theoretically calculated and experimentally determined limit-state stresses gives confidence in the characterization of the sand and testing methodology used in this study.

Active and Passive p-y Response under Cyclic Loading

In this section, the test setup will be used to measure the cyclic p-y response of the wall supporting medium dense sand. The top of the rigid wall was subjected to 40 cycles of lateral displacement, which were subdivided into four displacement intervals: $[\pm 2 \text{ mm}]$ (0.17 % drift), $[\pm 5 \text{ mm}]$ (0.41 % drift), $[\pm 10 \text{ mm}]$ (0.83 % drift), and $[\pm 20 \text{ mm}]$ (1.67 % drift). The cyclic testing program is summarized in [figure 24](#). Each displacement interval was cycled 10 times before moving to the higher interval. A complete cycle is defined by the distance the wall moves between two consecutive lower bounds of a given interval. A cycle consists of a passive wall movement followed by an active wall movement. When the number of cycles in a given interval was completed, the wall was moved to the lower bound of the next displacement interval and a new set of cycles is initiated. The first cycle in the new displacement interval is referred to as a transitional cycle. In [figure 24](#), transitional cycles are distinguished from the rest of the cycles within the same drift level by a heavy solid line because of their distinctive behavior.

It is worth noting that the primary loading scenario that is being modeled by the “cyclic loading” experiments is loading under earthquake cycles. However, it is clear that applying 10 “static” cycles whereby the wall is displaced back and forth between active and passive conditions does not simulate a real earthquake. Obviously, all effects related to inertia, viscosity, and damping are not being modeled in such a simple experiment. As a result, it could be considered that the primary objective of the cyclic tests is to investigate the effect of repetitive loading on the densification of the backfill and the resulting “static” p-y response. If considered from the perspective of rheological modeling in which the soil behind the wall is replaced by a simple “spring” and “dashpot” system, the cyclic tests in this study may be used to get better understanding of the response of the static spring stiffness under cyclic loading, with no information gained on the response of the dashpot. This is a limitation that could be addressed in future work.

[Figure 25](#) shows the p-y response recorded at Sensors #1, #2, and #3, respectively, as the rigid wall was cycled between the four displacement intervals described in [figure 24](#). The lateral movement at Sensor #4 was relatively small because of its proximity to the bottom hinge. As a result, the p-y response at that level showed a lot of irregularities and was excluded from the presented results. The limits of the distance traveled by each sensor are indicated in the figures by two vertical lines extending from the horizontal axis.

To put the results into perspective, the theoretical active and passive limit state pressures as computed from the theories of Coulomb (1776) and Liu, Xia, and Liang (2018) were calculated and superimposed in [figure 25](#). Comparison with the active experimental response is shown at the lower cyclic amplitudes (2 mm), whereas comparison with the passive response is shown at the highest cyclic amplitudes (20 mm). The active pressures recorded for the first cycle indicate an acceptable level of agreement with Coulomb’s theory. However, with increased number of cycles, the predicted active pressures overestimate the measured values. This is expected given that densification of the soil is expected to occur in the sand with repeated cyclic loading and unloading.

FIG. 24

Testing program for the cyclic loading of medium-dense sand.

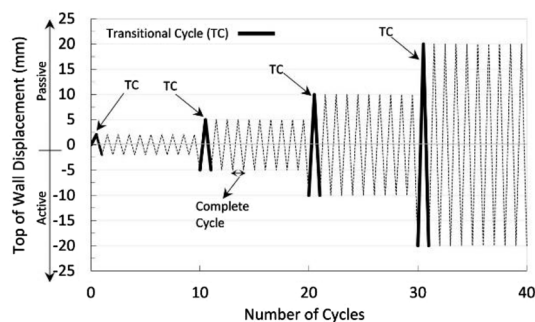
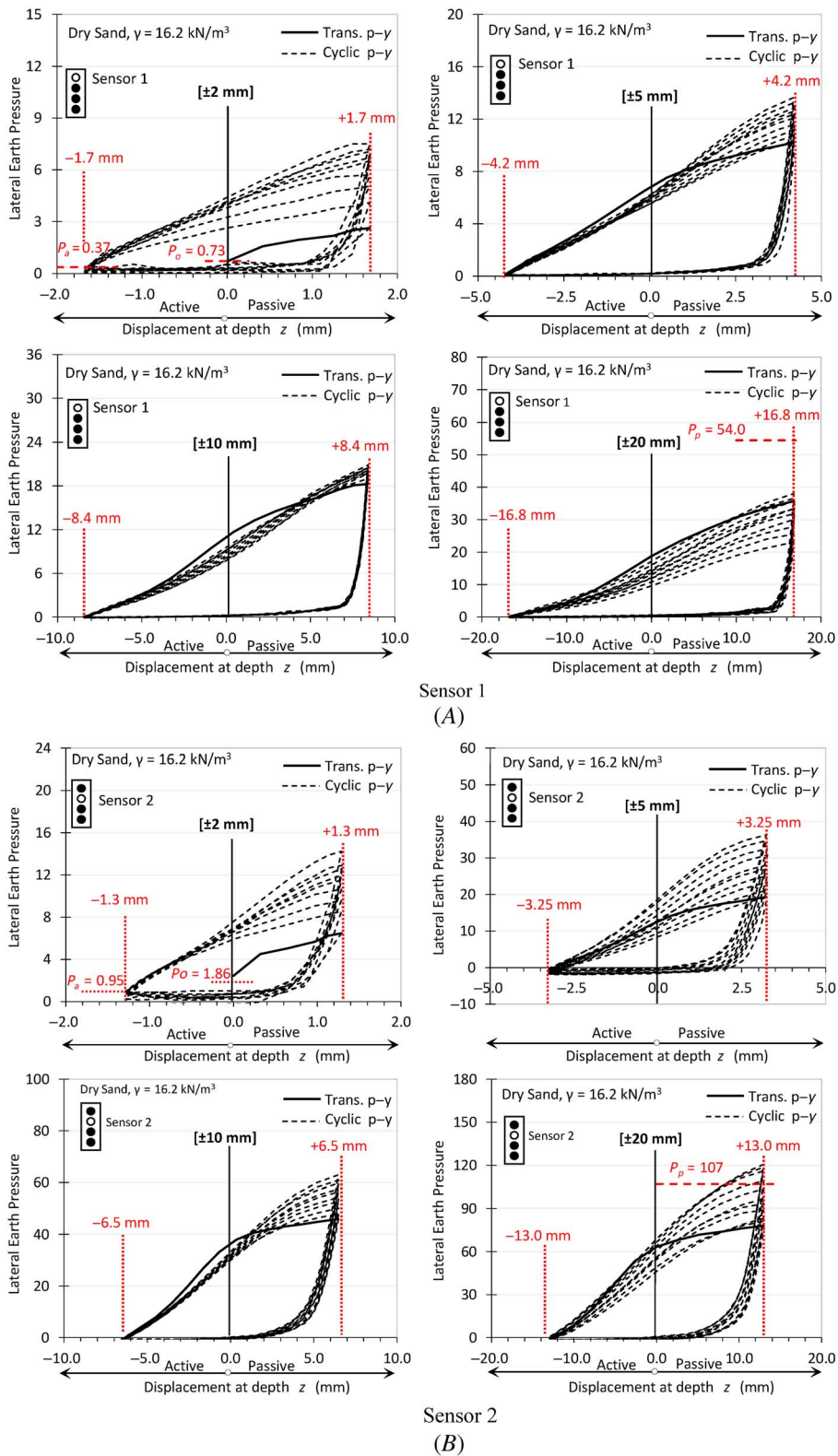
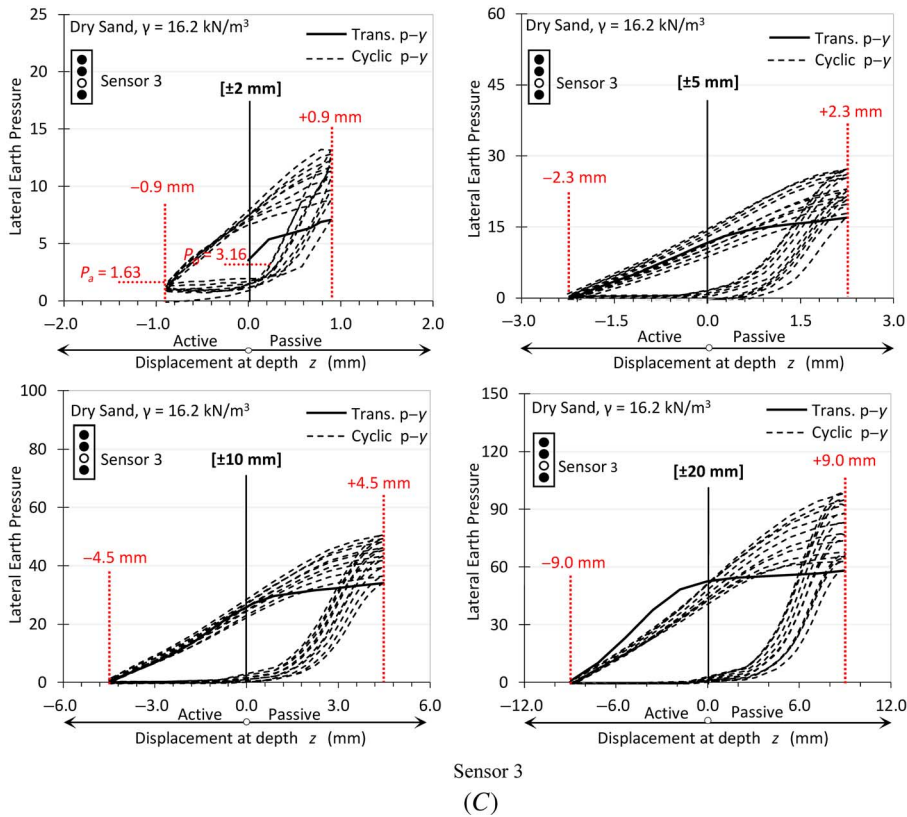


FIG. 25 Cyclic p-y response for the case of medium-dense soil for (A) Sensor 1, (B) Sensor 2, and (C) Sensor 3.



Downloaded from http://asmedigitalcollection.asme.org/geotechnical/article-pdf/46/1/104/7085199/10_1520_gj120220084.pdf by American University of Beirut Ab user on 09 April 2024

FIG. 25 Continued



The passive pressures at limit state as predicted by the log-spiral method proposed by Liu et al. (2018) method are plotted in figure 25 for the 20 mm displacement cycle. Results show that for the lateral stresses, Sensor #2 was the only sensor to have its peak pressures approach the limit-state passive pressure after several cycles. As for the rest of the sensors, their peak pressures fell shy of the limit state pressures. At Sensor #3, the calculate limit state pressure was located outside the figure scale and therefore could not be presented in the figure.

A closer look at the cyclic p-y response in figure 25 leads to several observations. First, the observed p-y curves that describe the response of the soil as the wall is moved in the passive and active directions are nonlinear for all magnitudes of displacement intervals. This observation is in line with finite element results presented in Elchiti et al. (2017) and El-Chiti et al. (2018) for the active response. This indicates that simple elastic-perfectly plastic p-y models may not be representative of the actual lateral earth pressure response of sands during cyclic loading.

Second, the results point to the importance of cyclic loading on the overall p-y response. At any given wall displacement in the passive direction, the lateral stress behind the wall is found to increase incrementally following each cycle. This holds true for the pressures recorded at Sensors #2 and #3. Sensor #1, on the other hand, behaved distinctively from other sensors at large displacement intervals. At ± 10 mm displacement interval, Sensor #1 maintained approximately the same peak pressures throughout the 10 cycles, whereas at ± 20 mm displacement interval, it experienced a drop in lateral pressures with increased number of cycles. This distinctive behavior is attributed to the low confinement depth at Sensor #1.

Third, an examination of the p-y response in the unloading portion of the p-y curves (passive side to active side) indicates that the lateral stress drops at a very fast rate as the direction of wall movement is reversed from passive to active. The rate of decrease in the lateral stress seems to be insensitive to the number of loading cycles

and to the magnitude of the peak pressure. This can be observed by highlighting the remarkable consistency of the unloading sections of the p-y curves between cycles. The shape of the active section of the p-y curve is “hyperbolic” and consistent with numerically derived curves as reported in El-Chiti et al. (2018). The transition from the “passive” to the “active” side is characterized by an initial sharp decrease in lateral stress followed by a gradual reduction in stiffness leading eventually to the mobilization of full active conditions behind the wall. It is interesting to note that the wall displacement required for the lateral stress to reach active conditions increases as the range of the displacement interval increases. For instance, at the location of Sensor #2, the wall displacement that is needed to reduce the maximum pressure to the active limit state pressure increases from about 1 mm for the 2 mm displacement cycles to around 10 mm for the 20 mm displacement cycles.

Fourth, the results show a clear difference between the response of the transitional p-y curve (the first loading curve in a new displacement interval) and the rest of the curves. Transitional passive p-y curves show an approximate bilinear p-y response (solid lines), whereas the rest of the p-y curves are represented by “S-shaped” curves. This difference in response could be attributed to the fact that the transitional p-y curve for any given interval is affected by the stiffness of the soil reached in the last cycle of the preceding interval (which has a smaller drift compared with that of the current interval). The “S-shaped” p-y response seems to become more defined as the range of the cyclic wall displacement is increased from 2 to 20 mm. It can be noted that the first p-y curve that follows the transitional p-y curve experiences a drop in passive soil stiffness (compared with the transitional curve). After that, gradual increases in stiffness are observed in the passive p-y curves of consecutive cycles. This gradual increase in stiffness seems to decrease as the number of cycles increases. Convergence in the passive stiffness was observed at the terminal displacement cycles (9 and 10 cycles) for almost all displacement intervals.

It is worth noting that the reduced stiffness that is exhibited in the transitional p-y curve could be explained by the shifting of Zone #3 (see [fig. 21](#)) to new regions of immobilized soil at the new drift level of wall displacement. This leads to the redefinition of zone boundaries resulting in a drop in passive soil stiffness in the following p-y curve. As for the rest of the passive p-y curves, a gradual increase in stiffness with each cycle is recorded because of densification, as indicated previously.

Conclusions

Based on the results of three static tests (three relative densities) that were conducted by displacing the wall from an at-rest condition to an active condition, followed by passive loading up to a maximum wall displacement of 10 % of the height of the wall (around 120 mm), the following conclusions can be made:

- At-rest to active p-y curves are relatively curved with an observed decrease in the rate of stress loss with increased wall displacement. The measured p-y response is sensitive to the active wall displacement with a top wall displacement of -8 mm being sufficient to reduce the lateral pressures from the at-rest to active pressure at all sensors.
- At-rest to passive p-y curves are characterized by a monotonic increase in lateral pressure with passive wall displacement. The responses are nonlinear in shape with varying intensity depending on the location/depth of the sensor and the magnitude of applied displacement. Among the four sensors, only the upper sensor recorded stresses that reached passive conditions. The stresses in the deeper sensors showed no signs of asymptotic behavior because of the relatively small wall displacements that were not large enough to induce nonlinearity in the p-y response.
- The effect of relative density on both the active and the passive p-y responses was significant. Loose sand was the slowest to approach the active limit state, with the amount of wall displacement required to mobilize active conditions for the case of loose soil (3 to 4 mm) being approximately 3.5 times that for medium-dense soil and 8.0 times that of dense soil. On the other hand, the passive response indicated that denser soils tend to exhibit stiffer p-y responses compared with looser soils.

Based on the cyclic p-y response of a wall supporting medium dense sand, the following conclusions can be made:

- Cyclic p-y curves that represent the mobilization of lateral earth pressure behind the rigid rotating wall are highly nonlinear and cannot be adequately represented by the simple elastic-perfectly plastic model that was adopted in the literature in modeling soil-structure interaction between basement walls and sand backfill.
- Because a process of densification that must have dominated the volumetric tendency of the sand behind the wall during cyclic loading, the p-y curves showed a significant increase in the maximum pressure at the passive side after 10 loading cycles. An observation of the initial stiffness that characterizes the p-y response in the passive direction also showed a gradual increase in stiffness with consecutive loading cycles. This gradual increase in stiffness decreased with the number of cycles until convergence in the passive stiffness was observed at the terminal displacement cycles (9 and 10 cycles) for almost all displacement intervals.
- Unlike the passive response, the p-y curves representing the unloading cycles (from passive to active) were insensitive to the cycled loading and showed remarkable consistency between cycles. However, it was observed that the displacement required for the lateral stress to drop from passive to active during the unloading cycle increased as the cyclic displacement interval increased.

Current p-y models that are adopted in numerical soil-structure-interaction modeling of basement walls in buildings with underground stories are based on simplified p-y curves (Briaud and Kim 1998) that are obtained from data from full scale tie-back walls. These backbone curves assume that active conditions are mobilized at a fixed displacement of 1.3 mm and the passive at 13 mm. Data collected in this study indicate that the passive p-y curves proposed by Briaud and Kim (1998) prematurely predict the occurrence of passive limit state pointing to the need for advanced p-y models that could better predict the p-y response. This study shows that p-y curves for rigid walls are not that simple to model because they depend on the soil density and depth below ground surface and, more importantly, are highly sensitive to cyclic loading.

It is clear that “scaling effects” need to be taken into account before generalizing the results of this experimental program to full-scale practical problems. The magnitude of the expected lateral stresses behind a full-scale basement wall will be relatively higher than the stress state in the intermediate-scale model experiments. However, intermediate-scale model tests (like the ones conducted in this study) that involve pressure sensors could provide valuable insight on the cyclic p-y response and its sensitivity to density and confinement. Results of intermediate-scale experimental tests could be used in future work to calibrate numerical models that would in turn be used to predict the response of full-scale basement walls under the true field stress conditions and to get additional insight to aid soil-structure-interaction modeling of buildings with underground stories.

References

- Briaud, J.-L. and N.-K. Kim. 1998. “Beam-Column Method for Tieback Walls.” *Journal of Geotechnical and Geoenvironmental Engineering* 124, no. 1 (October): 67–79. [https://doi.org/10.1061/\(ASCE\)1090-0241\(1998\)124:1\(67\)](https://doi.org/10.1061/(ASCE)1090-0241(1998)124:1(67))
- Coulomb, C. A. 1776. “Essai sur une application des règles de maximis et minimis à quelques problèmes de statique, relatifs à l’architecture.” *Memoires de Mathematique de l’Academie Royale de Science* 7: 343–382.
- Dave, T. N. and S. M. Dasaka. 2012. “Assessment of Portable Traveling Pluviator to Prepare Reconstituted Sand Specimens.” *Geomechanics and Engineering* 4, no. 2: 79–90. <https://doi.org/10.12989/gae.2012.4.2.079>
- El Ganainy, H. and M. H. El Naggar. 2009. “Seismic Performance of Three-Dimensional Frame Structures with Underground Stories.” *Soil Dynamics and Earthquake Engineering* 29, no. 9 (September): 1249–1261. <https://doi.org/10.1016/j.soildyn.2009.02.003>
- Elchiti, I., G. Saad, S. Najjar, and N. Nasreddine. 2017. “Investigation of Active Soil Pressures on Retaining Walls Using Finite Element Analyses.” In *Geotechnical Frontiers 2017: Walls and Slopes*, edited by T. L. Brandon and R. J. Valentine, 159–169. Reston, VA: American Society of Civil Engineers. <https://doi.org/10.1061/9780784480458.016>
- El-Chiti, I., G. Saad, S. S. Najjar, and S. Alzoer. 2018. “Numerically Derived P-Y Curves for Rigid Walls under Active Conditions.” In *Numerical Methods of Geotechnical Engineering IX: Proceedings of the Ninth European Conference on Numerical Methods in Geotechnical Engineering (NUMGE 2018), June 25–27, 2018, Porto, Portugal*, 1–8. London: CRC Press.
- Fang, Y.-S. and I. Ishibashi. 1986. “Static Earth Pressures with Various Wall Movements.” *Journal of Geotechnical Engineering* 112, no. 3 (March): 317–333. [https://doi.org/10.1061/\(ASCE\)0733-9410\(1986\)112:3\(317\)](https://doi.org/10.1061/(ASCE)0733-9410(1986)112:3(317))
- Fang, Y.-S., Y.-C. Ho, and T.-J. Chen. 2002. “Passive Earth Pressure with Critical State Concept.” *Journal of Geotechnical and Geoenvironmental Engineering* 128, no. 8 (August): 651–659. [https://doi.org/10.1061/\(ASCE\)1090-0241\(2002\)128:8\(651\)](https://doi.org/10.1061/(ASCE)1090-0241(2002)128:8(651))

- Fang, Y.-S., T.-J. Chen, R. D. Holtz, and W. F. Lee. 2003. "Reduction of Boundary Friction in Model Tests." *Geotechnical Testing Journal* 27, no. 1 (December): 3–12. <https://doi.org/10.1520/GTJ10812>
- Gutberlet, C., R. Katzenbach, and K. Hutter. 2013. "Experimental Investigation into the Influence of Stratification on the Passive Earth Pressures." *Acta Geotechnica* 8, no. 5 (October): 497–507. <https://doi.org/10.1007/s11440-013-0270-3>
- Khosravi, M. H., T. Pipatpongsa, and J. Takemura. 2013. "Experimental Analysis of Earth Pressure against Rigid Retaining Walls under Translation Mode." *Géotechnique* 63, no. 12 (September): 1020–1028. <https://doi.org/10.1680/geot.12.P.021>
- Lancellotta, R. 2002. "Analytical Solution of Passive Earth Pressure." *Géotechnique* 52, no. 8 (October): 617–619. <https://doi.org/10.1680/geot.2002.52.8.617>
- Liu, S., Y. Xia, and L. Liang. 2018. "A Modified Logarithmic Spiral Method for Determining Passive Earth Pressure." *Journal of Rock Mechanics and Geotechnical Engineering* 10, no. 6 (December): 1171–1182. <https://doi.org/10.1016/j.jrmge.2018.03.011>
- Matlock, H. 1970. "Correlations for Design of Laterally Loaded Piles in Soft Clay." In *The Offshore Technology Conference*, OTC-1204-MS. Houston, TX: Offshore Technology Conference. <https://doi.org/10.4043/1204-MS>
- Patel, S. and K. Deb. 2020. "Study of Active Earth Pressure behind a Vertical Retaining Wall Subjected to Rotation about the Base." *International Journal of Geomechanics* 20, no. 4: 04020028. [https://doi.org/10.1061/\(ASCE\)GM.1943-5622.0001639](https://doi.org/10.1061/(ASCE)GM.1943-5622.0001639)
- Reese, L. C., W. C. Cox, and F. D. Koop. 1974. "Analysis of Laterally Loaded Piles in Sand." In *The Sixth Annual Offshore Technology Conference*, OTC-2080-MS. Houston, TX: Offshore Technology Conference. <https://doi.org/10.4043/2080-MS>
- Richards, R., Jr., C. Huang, and K. L. Fishman. 1999. "Seismic Earth Pressure on Retaining Structures." *Journal of Geotechnical and Geoenvironmental Engineering* 125, no. 9 (September): 771–778. [https://doi.org/10.1061/\(ASCE\)1090-0241\(1999\)125:9\(771\)](https://doi.org/10.1061/(ASCE)1090-0241(1999)125:9(771))
- Saad, G., S. Najjar, and F. Saddik. 2016. "Seismic Performance of Reinforced Concrete Shear Wall Buildings with Underground Stories." *Earthquakes and Structures* 10, no. 4 (April): 965–988. <https://doi.org/10.12989/eas.2016.10.4.965>
- Tabaroei, A., S. Abrishami, and E. S. Hosseininia. 2017. "Comparison between Two Different Pluviation Setups of Sand Specimens." *Journal of Materials in Civil Engineering* 29, no. 10 (October): 04017157. [https://doi.org/10.1061/\(ASCE\)MT.1943-5533.0001985](https://doi.org/10.1061/(ASCE)MT.1943-5533.0001985)
- Take, W. A. and A. J. Valsangkar. 2001. "Earth Pressures on Unyielding Retaining Walls of Narrow Backfill Width." *Canadian Geotechnical Journal* 38, no. 6 (December): 1220–1230. <https://doi.org/10.1139/t01-063>
- Tatsuoka, F. and O. Haibara. 1985. "Shear Resistance between Sand and Smooth or Lubricated Surfaces." *Soil and Foundation* 25, no. 1 (March): 89–98. <https://doi.org/10.3208/sandf1972.25.89>
- Tsagareli, Z. V. 1965. "Experimental Investigation of the Pressure of a Loose Medium on Retaining Walls with a Vertical Back Face and Horizontal Backfill Surface." *Soil Mechanics and Foundation Engineering* 2, no. 4 (July): 197–200. <https://doi.org/10.1007/BF01706095>
- Yankelevsky, D. Z., M. Eisenberger, and M. A. Adin. 1989. "Analysis of Beams on Nonlinear Winkler Foundation." *Computers & Structures* 31, no. 2: 287–292. [https://doi.org/10.1016/0045-7949\(89\)90232-0](https://doi.org/10.1016/0045-7949(89)90232-0)